Design, Challenges, and Trends of Inductive Power Transfer Couplers for Electric Vehicles: A Review

Sampath Jayalath, *Member*, and Azeem Khan, *Senior Member, IEEE*

***Abstract*—The magnetic coupler is the heart of an inductive power transfer system, which facilitates wireless power transfer through its air gap. The couplers are designed to maximize efficiency, power density, power transfer distance, and misalignment tolerance while minimizing leakage flux, weight, cost, and volume. The coupler design process becomes complex due to the non-linear behavior of magnetics, sophisticated geometrical structures, and mandatory design limitations imposed by standards such as SAE J2954/1, IEC 61980-1:2015, and ISO 19363:2020. Initially, this paper reviews the advancements in coil design methodologies and their structures over the last few decades to identify the ongoing challenges and trends. The impact of the power electronics system, industrial standards, material selection, numerical and analytical modelling methods, and thermal modelling on the coil design process are identified to formalize the design procedure. A coil design example based on finite element analysis (FEA) tools is presented to identify the drawbacks of the existing design and optimization process. A sensitivity analysis, 3D-Pareto plots, and optimal design selection by considering misalignment variations are proposed to improve the multi-objective optimization process. A generalized guideline for coil design is proposed, which highlights essential design stages of an inductive power transfer (IPT) coupler. Current trends are identified, and future directions are proposed.**

***Index Terms*— electric vehicles (EV), IPT coils, passive shielding, stationary charging, wireless power transfer,**

I. Introduction

AUTONOMOUS EVs are the future of the transportation industry [1], where wireless power transfer (WPT) technology will improve operational flexibility as it replaces human interaction in traditional wired charging methods[2]. Galvanic isolation and spark-free operation of IPT systems will further enhance the safety aspects of charging EVs. IPT systems are used for both stationary and dynamic charging. Stationary charging is implemented in households and parking bays, while dynamic charging is implemented in roads and industrial environments where multiple transmitting coils are embedded in the ground [3]-[5]. Both systems have a single receiving coil in the EV. However, stationary charging systems offer better charging control and reliability over dynamic systems.

A typical stationary charging IPT system for an EV is shown in Fig. 1. It consists of subsystems such as a power factor correction (PFC) converter, inverter, coupler, filter, impedance matching network (IMN), rectifier, and impedance converter (Z-Conv). Current research on IPT technology focuses on enhancing these subsystems' performance in terms of improving the efficiency, reliability, and safety of IPT systems. The recent review articles on WPT aim to provide an overall view of the state of the art trends and challenges of this technology [2],[5]-[16]. However, the literature lacks an in-depth review and analysis of the advancement of coil structures for stationary IPT systems over the years and their design challenges. Therefore, this paper focuses on the coil design stage for stationary charging IPT systems.

Coil design can be considered as one of the critical aspects of an IPT system, as it contributes to performance benchmarks such as:

1. Minimum efficiency requirement;
2. Safety aspects related to mitigating leakage magnetic field;
3. Interoperability;
4. Misalignment performance;
5. Cost, volume and weight;

Limitations on these benchmarks are defined under standards such as SAE J2954/1[17], IEC 61980-1:2015 [18], ISO 19363:2020 [19]. Analytical and numerical methods are utilized to assess the design objectives mentioned above, while multi-objective optimization strategies are proposed to enhance their performance further.

The coils proposed for EV applications have complex shapes

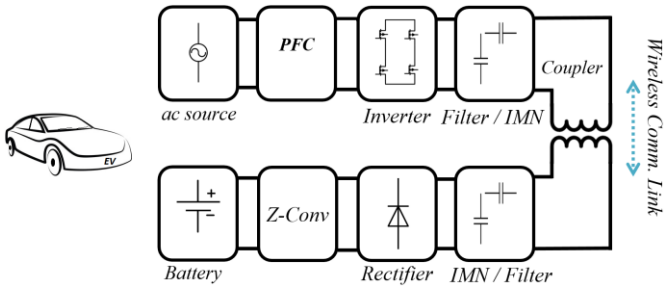

Fig. 1. Inductive power transfer system of an EV

Manuscript received August 04, 2020; revised October 12, 2020; accepted November 20, 2020. This work was supported in part by the University of Cape Town and National Research Foundation of South Africa.

The authors are with the Department od Electrical Engineering, University of Cape Town, Cape Town, 7700, South Africa (email: sampath.jayalath@uct.ac.za; azeem.khan@uct.ac.za)

and winding arrangements, making their design process a challenging task. Therefore, it is vital to have a detailed understanding of the following topics to improve the coil design process:

1. Advancements in coil design methodologies;
2. Evolution of coil geometries and configurations;
3. Coil design;

- Impact of Power Electronics system design
- Impact of industrial standards
- Material selection process
- Challenges in FEA based modeling methods;
- Challenges in optimization of couplers;

Therefore, this paper provides review and analysis on the topics mentioned above to define the state of the art of the coil structures, design methods, and identify the challenges related to it. The analysis presented is based on the FEA simulation tool due to the complexity of the study. However, the simulation results from these tools match well with the experimental results. Therefore, simulations are adequate for comparative analysis [20],[21]. Sensitivity analysis is proposed to reduce the number of design variables of a coupler to improve the optimization results and reduce computational time. 3-D Pareto plots are recommended as an alternative to 2-D plots to facilitate better decision making in selecting the best design through optimization. The importance of incorporating limitations of the power electronic system on the coil design is highlighted to improve the overall performance of the IPT system. This paper shows that the failure to incorporate misalignment scenarios during the design and optimization stage may result in a sub-optimum IPT system when considering its overall operation. Moreover, this paper proposes a generalized design guideline for any WPT coupler based on the review and analysis, which can be applied to any coil design problem. The paper concludes with future directions for IPT coupler designs.

II. Advancements in Coil Design Methodologies

The coil design methodologies evolved over the last few decades due to the advancements in analytical, numerical, and optimization techniques. In 1973, an IPT system to power an air-cored receiver coil of an EV through an air gap of 30 mm from two copper tubes in the transmitter was proposed by Otto[22]. However, the functionality of this system was not verified experimentally.

In 1997, Laouamer et al. introduced a pot core-based coupler for an IPT system to transfer 3 kW across an air gap of 6 to 8 mm. Litz wire was utilized for the winding to reduce skin effects, and the system was tested for a circular coil with ferrite cores[23]. Sakamoto et al. designed a two-winding circular coil structure with a thin ferrite plate and an iron plate for shielding. The coil structure parameters were extracted by simulating it in a magnetic field analysis tool (ELF MAGIC). The system was able to transfer 8.3 kW over an air gap of 3mm at 97% efficiency. The coupler's performance against the vertical, horizontal, and angular misalignment was also considered [24]. Nakao et al. investigated the concept of ferrite strips in the shape of fan-shaped bars to reduce the overall weight by 62.5 %, compared to conventional circular ferrite sheets with the coupling coefficient matching almost 90% to that of the conventional structure[25].

Mecke et al. proposed a circular coil (Litz wire) with a 200 mm radius to transfer power over an air gap of 300 mm. The coil was glued to ferrite plates to improve the flux linkage and coupling coefficient. Detailed analysis on selecting a suitable transmission frequency and sizing of the coils was also presented. Their IPT system operated at 100 kHz and transferred 1 kW of rated power at an efficiency greater than 80%[26].

The major drawbacks in all of these designs were that the coil parameters' optimum values were not identified to maximize or minimize an objective. The designer had lesser knowledge about the impact of coil parameters on the performance of the IPT system. Furthermore, no emphasis was given to limiting leakage magnetic fields to comply with safety standards [17]-[19], [27].

However, in 2011, Budhia et al. investigated the impact of each parameter of a circular coil structure by conducting extensive simulations using FEA to identify the limits of parameters such as the volume of ferrite material, angle of ferrite sectors, positioning of ferrite strips, number of turns, coil's inner and outer diameter, in improving the coil performance[28]. The misalignment performance and leakage magnetic flux density of the optimized coil were investigated to emphasize the need to comply with the ICNIRP 2010 standard in limiting leakage magnetic fields. This detailed analysis was capable of identifying the strength and limitations of a circular coil structure, which led to the exploration of alternative coil structures such as DD-coils [29],[30] , DDQ coils [29], bipolar coils [31],[32], tripolar coils [33]-[35] and, XPAD [36]. Detailed analysis on these coil structures is presented in section III. Parametric design studies similar to that of circular coils are also conducted for DD- coils [30] , DDQ coils[29], bipolar coils [31],[32] and tripolar coils [33]-[35]. Most of these studies search for the optimum parameter value for a single objective by keeping other parameters constant. Therefore, it may not result in an optimum design as the objectives are a function of multiple parameters, and increasing one parameter to reach an optimum will adversely affect the other objectives. However, with complex geometrical structures, this method may be a feasible solution to realize a sub-optimal design given the complexity and limitations in analytical and numerical modeling methods, as shown in section IV-D.

As a result, optimization based on Genetic algorithms were introduced to evaluate the coil performance with different parameter combinations [37],[38]. Furthermore, multi-objective optimization strategies were also considered to optimize the couplers for objectives such as maximizing coil-to-coil efficiency (η_c) [37]-[45], figure of merit (FOM) [41]-[43],[46] (k[47],[48] and Q[48]), power transfer capability [38],[40]-[44],[48], power density [45], minimizing leakage flux [39],[45], weight [42],[49], cost [47] and volume [40],[49]. A detailed discussion of these objectives is provided in section IV-A. Two dimensional (2D) Pareto-fronts are used to select the best design from multiple objectives[20][50]. In addition, individual components such as core shapes [51]-[53] and shields [54] are also optimized.

Design constraints must be incorporated into multi-objective optimization[20],[55]. For an IPT system, these constraints are

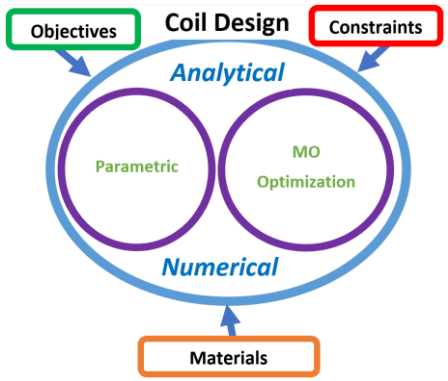

Fig. 2. Coil design process

the coil's size, power transfer distance, operating frequency, the temperature rise of the coil, and the power electronics (PE) system's limitations. Limitations of these constraints are discussed in section IV-B. The coil design process can be summarized, as shown in Fig. 2. The design process is facilitated by analytical and numerical methods, while the parametric and multi-objective optimization-based designing are subsets of it. The material selection, constraints, and objectives depend on the application and are input to the design process.

However, failure to consider these limitations during multi-objective optimization and may result in a suboptimum IPT system. It will be shown in Fig. 12 (c) that some designs become invalid when constraints are taken into consideration.

In literature, the optimization problem formulation lacks formality. The parameters to optimize vary from one solution to another, as seen from the designs listed under Table I for coils. Therefore, this paper proposes sensitivity analysis, as shown in section V. It is used to identify the critical parameters and improve the optimization's effectiveness by reducing the number of parameters. Moreover, the selected modeling methods are critical during optimization. Some methods are not appropriate for the considered optimization problem, as shown in section IV-D and V. It shows that the lack of space between coil-turns leads to different results and impacts the overall optimized solution.

A multi-objective optimization process utilizes a Pareto-front concept to determine the best design. As shown in section V, three-dimensional (3D) Pareto fronts are proposed, instead of 2D Pareto-fronts, to improve the decision making process in selecting an optimum design [20],[42],[50],[56].

The coils are often optimized to improve performance at the nominal position without considering the impact of misalignments on the coupler's overall performance. Therefore, the resulting design may not be fully optimum under misalignment conditions and violate design constraints shown

TABLE I
PROPOSED DESIGN AND OPTIMIZATION SOLUTIONS FOR IPT PADS

Type	Ref	Parameters	Constraints	Objectives	Methodology	Notes
Circular	[20]	$(D_c=2r_o)$, $(A_c=\pi r_c^2)$, f^{**}	T^{++}	η_c, α_A	Derivation of PF using FEA and Analytical	$^{**}f$-frequency, ^{++}T- Temperature
	[40]	N, r_i , r_c, CT	P, f, RS, h, N, $(A_c=\pi r_c^2)$	$P\eta_c$ vs f, P_o vs $P\eta_c$, h vs RS,	NSGA-II to derive PF	CT- Compensation topology, f-frequency, h-transfer distance, RS- Radial space footprint, $P\eta_c$- Power efficiency
	[48]	N, r_c , h_{wf}	r_o, P^{**}, I^*	k and Q	NSGA-II to derive PF, Optimization simulation for 100 generations, 50 individual problems	$^{**}P$- Power transferred, and I^*- coil currents< saturation current.
	[63]	N^*, r_i , r_o	NA	η_c, B_s	Lump loop model to derive PF, ten simulations are required for entire optimization	$^*N$-Turn distribution, Fe size, gap and misalignment are fixed parameters.
	[88]	d_s, $(2r_o)$, w_c, $(2r_c)$,N_T,d_{if} , l_f, w_f, N_f, f, and I_1	d_s, B_s, CL	P_T, C_T, D_h	NSGA-II to derive PF, 104 simulations.	d_{if}- internal diameter of Fe ends, f-frequency, I_1-primary current, P_T- Total loss, C_T- total cost, D_h- horizontal misalignment tolerance, CL- converter limitations
DD	[45]	L_c, W_c,w_i,w_o, N_f, d_c	N^{**}	η_c, α_A, α_G, B_s	Derivation of PF using FEA and Analytical	Ferrite dimensions are unchanged, $^{**}L$-Number of turns are adjusted to fulfill design rules
	[65]	N, (2^*r_c),N_f, L_f, w_f, t_f, g_f, W_i , L_i	J, k_{bi}, $B_{c,m}$,$B_{c,a}$, P_{cd} and η_c>93%	η_c, α_A, α_G, $M_P{}^*$	PSO algorithm, Optimal PF	W_i and L_i are inner width and length of the coil
	[72]	(L_c/W_c), (w_i/L_c), N	NA	η_c, P	Parametric	$w_i=N_*$pitch, P-Power capacity, Shape of the Fe core is optimized.
DDQ	[65]	N_{DD}, N_Q, (2^*r_c),N_f, L_f, w_f, t_f, g_f, L_{iDD},L_{iQ} , $W_{i\,DD}$, W_{iQ}	J, k_{bi}, $B_{c,m}$,$B_{c,a}$, P_{cd} and η_c>93%	η_c, α_A, α_G, $M_P{}^*$	PSO algorithm, Optimal PF	L_{iDD}, L_{iQ} ,W_{iDD}, W_{iQ} are inner lengths and widths of the DD and Q coils, N_{DD}, N_Q are the number of turns of the DD and Q coil
	[73]	L_c, W_c, r_c, $L_Q=W_Q$, $(L_Q\text{-}2\ w_Q)^*$, N	L_M, I_1	k and P_{su}	Parametric	$L_Q{}^*$ Inner length of the Q coil, L_M- Mutual inductance, I_1-primary rms current
BBP	[31]	O_{LB}, w_c, L_f, N_f, w_f, t_f T_c, x_p, y_p, y_{cs}, x_{cs}, g_f, t_s,	Geometrical constraints (dimensions)	P_{su}	NA	x_{cs} , y_{cs}- gap between Fe and the winding, x_p , y_p – gap between winding and shield boundary
TPP	[33]	D_{oT}, w_{iT}, D_{cT},w_{oT}, O_{LT}, t_s, t_f, T_1, T_2, $h_{wf}=h_{fs}$	Geometrical constraints (dimensions)	k	Custom search algorithm	Dimensions to match CP and BPP used in [21], optimization of primary current to maximize effective coupling coefficient.

PF- Pareto front, η_c -coil to coil efficiency, B_s -leakage field, M_P – misalignment performance, k_{bi}-bifurcation factor, $B_{c,m}$-maximum core flux density ,$B_{c,a}$-average core flux density, P_{cd}-core loss density, P_{su}- Maximum uncompensated power, J- current density of the winding, α_A and α_G are area and gravimetric power density.

in section V. Therefore, the impact of misalignments must be incorporated into the design stage of the IPT couplers.

However, the performance improvements through optimization techniques are restricted by the design limitations, which are unique to different couplers. The following section will analyze coupler structures' advancements over the last decade to identify the key features that led to new geometries and configurations.

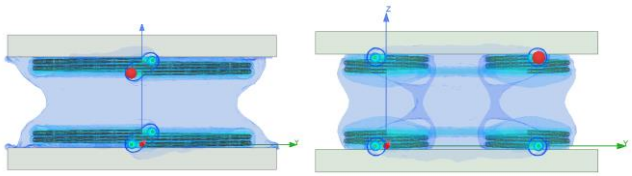

(a) (b)

Fig. 3. Magnetic field distribution of E and C types cores

III. Evolution of Coil Geometries and Configurations

The coil designs proposed in literature consists of complex coil arrangements with different geometries, conductive, and ferromagnetic elements. The Faraday and Biot Savart laws explain the fundamentals associated with the IPT coils [57]. The concept of the reluctance path of conventional single-phase power transformers can be used to understand the coil geometries' field distribution [45]. They are classified into E-type (reluctance path corresponding to two loops of conventional E or pot-core-based transformers) and C type (reluctance path corresponding to a single loop of the conventional toroid and C-core based transformers) IPT coils[45]. The field distribution of the E-type and C-type IPT coils is shown in Fig. 3. The field lines in E-type geometry that extend to both sides of the cores experience a similar reluctance to that of the direct field lines. This is due to the increasing magnetic cross-section, and the reluctance is inversely proportional to the magnetic cross-section and directly proportional to the path length. However, the flux is surrounded

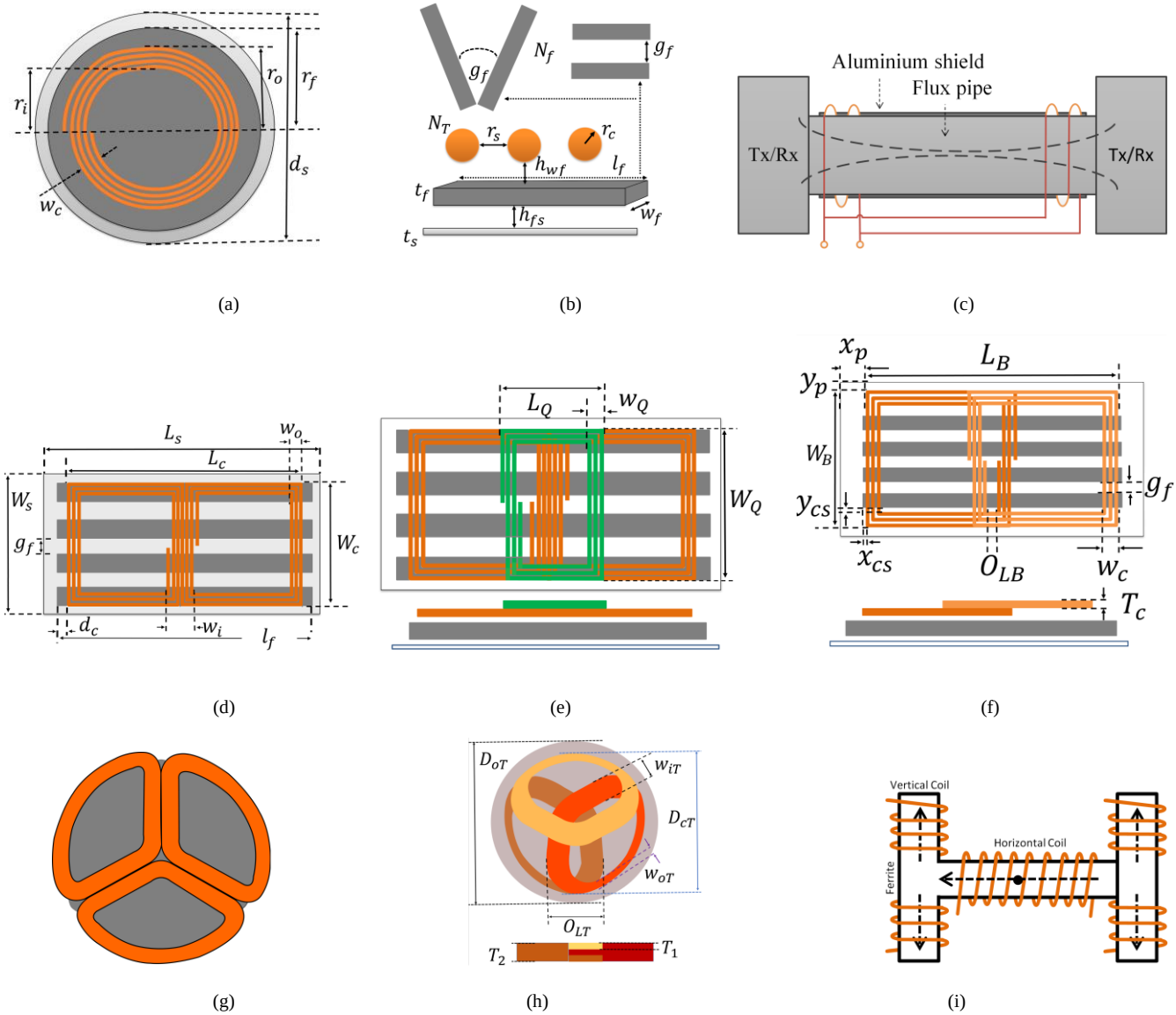

(a) (b) (c)

(d) (e) (f)

(g) (h) (i)

Fig. 4. 2D view of coil structures: (a). Circular pad [28], (b). Cores, shield, and winding or turns, (c). Flux pipe[68], (d). DDP [29], (e). DDQP [29], (f). BBP [31], (g).Trifoliate Pad [76], (h).TPP [33], (i). XPAD [36].

by the environment in E-type, as seen in Fig. 3(a), and it is a part of the magnetic circuit. On the other hand, there are two coils connected in series in C type, as seen in Fig. 3(b), and the flux is at opposite orientation at each side of the two transmitter coils. In this configuration, the magnetic field and reluctance path are contained within the coupler, and the environment is no longer a part of the magnetic circuit. Therefore, it is evident that the C-type couplers should have less magnetic stray field compared to E-type couplers [45]. The coil structures presented in the literature are classified according to E and C-types' magnetic field distribution, as listed in Table II. The 2D views of coil structures proposed for EVs are shown in Fig. 4. It is important to notice that a magnetic core is an integral part of the proposed coil structures to improve the coupling to the secondary coil while a passive shield reduces the leakage magnetic field and improves the structural rigidity of the coil.

A. Circular Pad (CP)

The CP can be identified as the frequently researched coil structure for EVs [13],[20],[28],[37]-[39],[43],[46],[48],[54],[56],[58]- [65]. The CP is shown in Fig. 4 (a). The parameters considered during the design and optimization of the CP are as follows: the number of turns (N_T), coil width (w_c), the radius of the copper(Cu) conductor (r_c), inner (r_i), and outer (r_o) radius of the coil, the diameter of the shield (d_s), the radius of the circular ferrite (Fe) block (r_f), Fe thickness(t_f), the thickness of the passive shield (t_s), the separation between Cu conductors (r_s), the separation between Cu conductor and Fe (h_{wf}), the separation between Fe and shield (h_{fs}). Fe bars are used instead of a circular ferrite blocks to reduce the pad's cost and weight, as shown in Fig. 4(b). Therefore, the number of Fe blocks (N_f), Fe length(l_f), Fe width(w_f), and the gap between Fe blocks (g_f) in degrees or millimeters are additional parameters of it. The parameters such as N_T, N_f, t_f, l_f, w_f, t_s, h_{wf}, h_{fs}, r_s, w_c, and r_c are common to coils such as DD, DDQ, bipolar and tripolar pads and are shown in Fig. 4(b).

The CP generates and couple perpendicular flux and the flux distribution is symmetrical around the coil center. Therefore, the magnetic core is placed symmetrically around the center of the coil to enhance coupling. Ferrite bars are employed instead of circular ferrite block to reduce weight, cost, and improve reliability. The tradeoffs between the number of ferrite bars and the coupling coefficient are studied in [28]. Table I lists down the recently proposed multi-objective optimization solutions for CP, and N, r_i, and r_o are the frequently optimized circular coil parameters. The general characteristics of circular couplers are,

a) Capable of transferring power across an air gap of (1/4) of their diameter [28];
b) Inner (r_i) and outer (r_o) radii are the main parameters responsible for magnetic coupling [20];
c) Power null occurs when the horizontal offset is around 40% of the coil diameter for similar transmitter and receiver coils [28];
d) It has equal misalignment tolerance in all directions [28].

CP provides a higher magnetic coupling than square and rectangular pads (RP) with a similar area [20]. It implies higher transmission efficiencies for the same area related power density of the pad [20]. However, square-shaped structures are preferred over circular structures in specific applications, as discussed in [66]. CP uses less material than the rectangular, solenoid, DD, and bipolar pads, transferring the same power over an air gap of 20 cm and 20 cm misalignment in the x and y-axis [67].

The circular coupler's main drawback is its limitation in power transfer distance compared to the coil's size and moderate tolerance towards misalignments [28]. It has poor interoperability performance with any coupler which produces polarized parallel flux (Eg: DD) as it couples perpendicular flux. The coil structures based on the concept of flux pipes are introduced to improve the coupling coefficient, as shown in Fig. 4 (c) [68]. However, the coil in Fig. 4(c) has a lower quality factor as the flux pipe generates a two-sided flux. Flux interacts with the passive shield and results in higher eddy current losses. Therefore, the efficiency of the charging drops. The horizontal flux produced by the coil ends is higher in magnitude and raises concerns over meeting the leakage flux limitations [7]. Therefore, the DD pad is proposed as a solution.

TABLE II
PROPERTIES OF COIL STRUCTURES

Coil Structure	Field Distribution	Flux direction	Flux pattern	System complexity	Interoperability (When used as a Tx)	Misalignment tolerance	Leakage field exposure with similar Rx
Circular	E-type	Single sided	NP	Simple	Poor with DD	Weak	Medium
Rectangular	E-type	Single sided	NP	Simple	Poor	Weak	Medium
Flux pipe	C-type	Double sided	P	Simple	Moderate	Moderate	High
DD	C-type	Single sided	P	Simple	Poor with Circular	Moderate	Low
DD-Q	C/E-type	Single sided	NP/ P	Complex	Good with all	Moderate	Low
Bipolar	C/E-type	Single sided	NP/ P	Complex	Good with all	Moderate	Low
Tripolar	C/E-type	Single sided	NP/ P	Complex	Good with all	Very good	Low
XPAD	C-type	Single-sided	P	Complex	Moderate	Moderate	Medium

*NP –Non-polarized, P-polarized, Tx- Transmitter, Rx- Receiver

B. DD Pad (DDP)

The DDP and its parameters are shown in Fig. 4 (d), The DDP utilizes the advantages of both the circular coil structure and the flux pipe concept to realize a single-sided flux path with height approximately half of the coil length [13],[29],[42],[44],[45],[47],[53],[69]. The parameters considered during the design and optimization of the DDP are as follows: outer width or spreading of the Cu winding($w_o=N*r_c+(N-1)*r_s$), inner width or spreading of Cu winding (w_i), the position of winding on the core (d_c), length(L_c) and width(W_c) of the coil, length(L_s) and width(W_s) of the shield, gap between Fe bars in *mm* (g_f). DDP generates and couples parallel flux polarized along the length of the coil. Therefore, the core is extended along the length of the coil to enhance coupling. Table I lists down the frequently optimized parameters for the DDP. The w_i is a critical parameter that affects the coupling coefficient. A smaller width results in lower reluctance between the two coils of the DDP due to the reduction in the magnetic path length and, consequently, a low coupling coefficient [45].

The two coils are connected magnetically in series, and the flux from one coil interacts with the other. Therefore, they are driven by a single power supply. However, in certain applications where DDP is used as the primary, the two coils are driven separately with two power supplies to obtain various field patterns at the expense of complex control due to mutual coupling between them[70].

It has lower leakage flux, reduced losses in the passive shield, and inherits C-type IPT configuration, as discussed above. The charging zone of DDP is enhanced by five times compared to the square with similar material cost [29]. The shielding of the DDP can be enhanced by extending the core on both sides to exceed the coil coverage to attracts the leakage flux [71]. Furthermore, the traditional bar core structure shown in Fig. 4(d) is modified to E-shaped cores with a central depressed transmitter coil to reduce the leakage field [72]. However, shielding properties are improved at the expense of additional ferrite. The losses of a traditional bar or block-based cores are high due to non-uniform flux density. Therefore, the thickness of the core is reduced linearly from the central region [53]. The core losses are reduced by more than 20% compared to the traditional bar and block core.

DDP has a weak interoperability performance with CP, as discussed section III-A. The DDP-DDP system has a coupling null when the horizontal offset is around ~34% of the coil length (in the *x*-axis direction), which results in low induced voltage due to lower flux interaction [29]. However, a quadrature (Q) coil is introduced to improve the x-axis performance.

C. DDQ Pad

A quadrature coil, is introduced to the DDP to improve the misalignment performance, as shown in Fig. 4 (e) [13],[29],[32], [66]. The quadrature(Q) coil is magnetically decoupled from the DDP and independently tuned to couple with the flux in the x-axis direction. In addition to the parameters considered for the DDP, the parameters of Q coil are the length (L_Q) and width of the coil (W_Q) and the spread of the copper winding (w_Q). The constant coupling can be achieved over a larger area by increasing the Q coil's bending radius to become circular-shaped compared to a conventional rectangular shaped coil. [73]. Table I lists down the frequently optimized parameters for DDQP.

The introduction of the quadrature coil will complicate the PE system and control as it requires two synchronized inverters (*Tx*-coil) or rectifiers (*Rx*-coil), depending on whether it is used as an *Rx* or *Tx* coil. The Q and DD coil can be driven separately to produce a nonpolarized perpendicular flux pattern or polarized parallel field pattern depending on the receiver pad. Both coils can also be driven simultaneously to generate a mix of perpendicular-parallel field pattern. The net field will be asymmetrical, and its dominating side (right or left side from the center of the DDQP) depends whether they are driven in phase or out of phase by 180^0. The ratio between the DD and Q coils' inductances determines the dominating field pattern (parallel or perpendicular). Furthermore, a moving magnetic field is generated by driving the Q coil with 90 out of phase compared to DD coil[70].

DDQP is frequently used as the receiver with the DDP transmitter as the DDP produces the desired flux pattern and Q coil in the DDQP receiver couples flux when the horizontal offset has an x-axis component [29]. Therefore, it eliminates the low coupling of DDP-DDP during misalignment. The charging zone of DDP-DDQP system is three times larger than a DDP-DDP system and five times larger than a CP-CP system with similar material cost and smaller size compared to CP-CP [70]. The DDQP is fully interoperable with CP compared to DDP due to the Q coil, as it generates perpendicular flux. Furthermore, the charging zone of a CP-DDQP is almost three times larger than a CP-CP[70].

The overall coil coverage of DDQP is almost similar to DDP or BBP coils but has higher copper utilization due to the quadrature coil. Therefore, bipolar pad is proposed to reduce copper utilization.

D. *Bi-Polar Pad* (BPP)

This configuration comprises two mutually decoupled D coils that partially overlap to form a BPP [13],[31],[32],[74],[75]. The structure is shown in Fig. 4 (f). The separation between the two coils is adjusted accordingly to achieve zero net flux linkage between them. Therefore, the overlap between the two coils (O_{LB}) is a critical parameter for BPP coil design. The other parameters are shown in Fig. 4(f). The copper utilization is considerably reduced compared to DDQ pads. The BPP is sensitive to horizontal flux, vertical flux, or both. Since the two coils are mutually decoupled, the BBP can be energized with different magnitudes and phases, depending on the receiver coil to achieve interoperability. The two coils in BPP can be driven in different modes by varying the primary current's magnitude and phase to generate different magnetic flux required to couple with different receiver pads. These coils can be driven in-phase, one coil at a time, 90^0 out of phase, and 180^0 out of phase. A non-polarized perpendicular flux pattern is generated if coils are driven-in phase (mode 1) while a parallel field polarized along the length of the coil is produced if driven out-of-phase by 180° (mode 2) [70]. However, a moving magnetic field is generated if driven with currents out-of-phase by 90° (mode 3). The coils in BPP can also be driven independently to produce a field neither perpendicular nor parallel (mode 4). IPT system shows a higher

tolerance to misalignment when coils are driven mode 3 operation compared to in-phase operation[31]. Similar to DDQP, it requires multiple converters and flux sensors, which complicate the control and operation. The BPP is sensitive to angular misalignment like any other polarized pad, and the coupling factor drops by 13% within a misalignment of 30 degrees [75]. The BPP as a transmitter is preferred over DDQP with a similar area due to their improved performance with lateral misalignment when used with DDP and CP secondary [70].

A trifoliate coil is a multi-winding coil structure proposed by Matsumoto et al.[76], as shown in Fig. 4 (g). Here three coils are connected in a "Y" configuration so that a three-phase inverter can drive it. It can achieve balanced electrical behavior between three phases at winding alignment and also balanced inductances between the windings. The trifoliate coil is the foundation for the development of the tripolar pad. The tripolar pad is proposed to improve the rotational tolerance of power transfer.

E. Tri-Polar Pad

The tripolar pad (TPP) consists of three mutually decoupled coils, which are partially overlapping with each other, as shown in Fig. 4 (h)[33]-[35]. The parameters of the TPP are the overlap between two adjacent coils (O_{LT}), the diameter of the coil structure (D_{cT}), the inner width of the winding (w_{iT}), the outer width of the winding (w_{oT}), the diameter of the magnetic core(D_{oT}) and different winding thicknesses (T_1 and T_2). It is also possible to realize a square-shaped TPP[33]. The mutual decoupling between coils is determined by the amount of partial overall between the three coils, and it is achieved by energizing one coil and adjusting the gap between the energized coil and the adjacent coil to ensure that the net electromotive force induced in an adjacent coil is zero[33]. It is critical to realize mutual decoupling between coils to minimize the VA required to drive the primary coils, reduce the losses, leakage magnetic field for given output power. However, small mutual coupling between the coils exists during the misalignment of the secondary coil due to the change in magnetic field path [33].

The three coils are driven individually with three separate inverters to maximize the power transfer capability (coupling coefficient), misalignment performance and, minimize leakage flux generated at the expense of an increase in control complexity and cost. The effective coupling coefficient between the TPP primary with the secondary coils such as CP and BPP can be effectively maximized by driving the individual coils with different magnitudes and phases[33].

The BPP has two mutually decoupled coils forming two poles, in which the direction of the magnetic field is from one pole to another. However, TPP has three mutually decoupled coils, which can also be driven in or out of phase with respect to each other. Therefore, the polarized magnetic field expands to multiple directions due to three mutually decoupled coils.

The TPP primary can transfer the same uncompensated power, with significant primary apparent-power (VA) reduction compared to CP [33]. The TPP-TPP coupler's performance is compared with the CP-CP with similar copper, ferrite, and aluminum in [34]. The coupling coefficient variation due to the misalignment of a TPP-TPP coupler is much lesser than a CP-CP system. Furthermore, the leakage field in TPP-TPP coupler is less compared to CP-CP for all the misalignment cases. Another study was conducted to compare the rotational misalignment tolerance TPP, BPP, and CP primaries with BPP secondary in terms of uncompensated power output [35]. The primary pads are driven at 40 kVA. The TPP primary maintained a high level of uncompensated power compared to BPP and CP primary when the BPP was rotationally displaced around the center of the primary coils.

Bipolar and Tripolar coils can be classified as multi-coils. Quadrupole [77] and triangular DQ coils are other examples of it [77]-[81]. They possess superior interoperability and misalignment performances than single-coils such as CP and DDP but at the expense of complex power electronics systems and control. A detailed performance comparison can be found in [79].

F. XPAD (Hybrid solenoid coupler)

The XPAD configuration is an improved version of the solenoid coil structure shown in Fig. 4 (c), which aims to reduce the flux leakage of a conventional solenoid coil, whilst maintaining an acceptable coupling[36]. As shown in Fig. 4 (i), it consists of a conventional solenoid and two series-connected orthogonal solenoids to direct the flux in the upward direction. Orthogonal solenoids mitigate the unwanted flux from the central solenoid. The performance of XPAD is compared with the DDP by having a DDP as the secondary coil. The outer dimensions, operating conditions, and the number of turns of the DDP are similar to the XPAD**.** The XPAD has a higher coupling coefficient than DDP, while the leakage magnetic field is higher in XPAD, compared to DDP. Furthermore, the primary current in XPAD is 50% less than the DDP due to a lower VA rating and inductance.

G. Intermediate-multi-coil

Intermediate coils are proposed to improve the coupling coefficient, transfer distance, and operating frequency range compared to two coil WPT systems [82],[83]. The increase in the coupling coefficient improves the efficiency of the system. The system proposed in [83] has a lower number of turns in the primary coil and reduced RMS current than systems with conventional two coil systems with equal power transfer.

H. Three-phase bipolar winding pad (TPBP)

The trifoliate coil and tri-polar coil discussed in section III-D and E are examples of three-phase coupler topologies with unipolar windings proposed for EV. The TPBP is proposed to increase power transfer capability and high-power density for high-power EV applications [84]. Fig. 5 shows TPBP proposed for EVs [84]. All the couplers have three winding pairs, and each pair is opposite in polarity. The flux produced in one coil has a natural return path through its opposite polarity coil. It can be seen from Fig.5 that the coil pitch and number of layers differ in each design presented, and the coil pitch must be less than the $nx60^0$, where n is the number of layers. The self-inductance of windings of different layers varies as they are located at a different distance from the ferrite plate, and mutual inductance between any two-phase windings also varies and depends on the layer, which each pair is located. However, interphase mutual inductance poses challenges in the system's operation

with large translational misalignment of the transmitter and receiver [84].

I. Discussion

Table I **s**ummarizes the parameters, constraints, objectives, and design methodology (optimization techniques and algorithms) used by various IPT pads proposed in the literature. The parameters and constraints choose to optimize vary from the designer to designer for a given coil structure, and less emphasis is given to parameters such as h_{wf}, h_{fs}, r_c, which becomes critical for thermal performances of a coupler[85]. These parameters are common to most of the coil structures. The 2D Pareto fronts are frequently utilized with all the optimization problems since multiple objectives are considered. Evolution algorithms such as GA and PSO are preferred to derive the Pareto-fronts of the design. Non-dominated Sorting Genetic Algorithm II (NSGA II) is a variant of GA, which shows excellent performance in searching the global optimal solution for nonlinear problems [40]. NSGA II is frequently used for the optimization of CP. However, these solutions are computationally expensive due to the significant number of FEA simulations during optimization. The CP is optimized based on lump loop models to reduce the computational cost, requiring only ten simulations[63]. However, a limited number of parameters are considered for optimization and may not be practical with complex coil structures**.** Section VI suggests some of the possible improvements in coupler optimization.

Table II summarizes some of the properties of the coils proposed in the literature. Most of the proposed coils generate single-sided flux. The double-sided flux coils tend to produce a higher leakage field as in flux pipe, which are not desirable for EV applications. Non-polarized coils are characterized by a single pole, while polarized coils have multiple poles within the structure. Polarized pads outperform non-polarized pads due to their ability to produce perpendicular flux, horizontally directed flux, and a field neither perpendicular nor parallel. Therefore, polarized coils show good tolerance to misalignments. However, non-polarized coils such as circular coil exhibit equal misalignment tolerance. The leakage field exposure can be roughly estimated based on the E-type and C-type field distribution and flux direction of the pads.

In the literature, several studies were carried out to evaluate coil performance for EV applications. Lin et al. provided an extensive comparison on pads such as CP, BPP, and solenoid pad (SP) for various primary and secondary coil areas. The comparison utilizes identical copper turn ratios and similar ferrite volumes for coils [21]. Table III summarizes some of the findings where couplers are categorized in descending order for the considered property. The coupling coefficients (k) listed in the Table III are for a primary coil design for a maximum area 0.36 m^2 to a secondary coil with a maximum area of 0.07m^2 at an 80 mm air gap for an above-ground charging scenario. BPP-SP has the highest coupling, while the SP-CP has the lowest. Similarly, maximum coupling coefficient variation due to misalignment(Δk), maximum magnetic efficiency (Eff), leakage field (B_L) at nominal and maximum misalignments at an air gap of 170mm are also listed in Table III. The highest k and the largest variation in k are observed for BPP: SP. The BPP as a primary have the maximum efficiency and reduced leakage field and interoperable with the other pad structures. The CP as a primary shows improved leakage field compared to BPP except for CP: SP. However, CP and DDP show weak interoperability characteristics since CP generates perpendicular flux, and DDP generates parallel flux polarized along the coil's length. The DDP performs poorly compared to DDQP and BPP in terms of interoperability due to its inherent mutually coupled structure, resulting in flux cancellation under some operating conditions [70]. Therefore, CP and DDP are not suitable for the primary operation. The BPP is fully interoperable with all the pads and shows excellent performance in leakage magnetic field and efficiency. Therefore, BPP is a strong candidate to be used as the primary pad. However, the leakage field of BBP is higher than DDQP[70], and BPP-BPP has weak rotational performance compared to TPP-BPP, as highlighted in Section III-E. DDQP and BPP outperform the CP and DDP when used as a secondary. However, both DDQP and BPP require two rectifiers and sophisticated controlling compared to CP and DDP, which requires a single rectifier[70].

It can be concluded that the important features of a coupler design are the pattern and intensity of its generated magnetic flux. The generated magnetic flux pattern depends on the coil geometry and the winding arrangement, which in turn, relates to its intensity. The coupling coefficient, mutual inductance, power transfer distance, efficiency, power density, leakage magnetic field, misalignment performance, and interoperability are functions of the generated magnetic flux. The environment

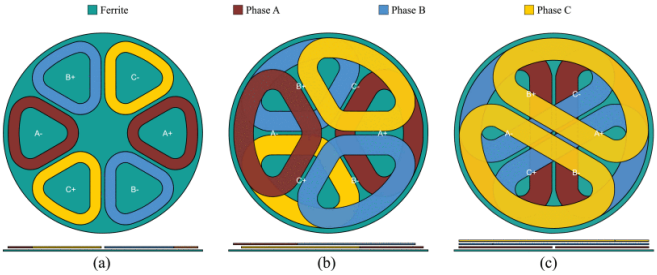

Fig. 5. Three-phase bipolar winding coils [84].

TABLE III
COMPARISON OF DIFFERENT COIL COMBINATIONS [21]

	k (@80mm)	Δk (@80mm)	Eff (%)	B_L (0,0)	B_L (150,150)
H	BPP:SP	BPP-SP	BPP-SP	SP-CP	SP-CP
	SP-SP	CP-SP	BPP-BPP	CP-SP	SP-SP
	BPP-BPP	BPP-BPP	BPP-CP	SP-SP	CP-SP
	CP-SP	SP-SP	CP-SP	SP-BPP	SP-BPP
	BPP-CP	BPP-CP	CP-BPP	BPP-SP	BPP-SP
	SP-BPP	CP-CP	CP-CP	BPP-BPP	BPP-CP
	CP-BPP	SP-CP	SP-SP	CP-BPP	BPP-BPP
	CP-CP	CP-BPP	SP-BPP	BPP-CP	CP-CP
L	SP-CP	SP-BPP	SP-CP	CP-CP	CP-BPP

**H and L- Coupler corresponding to highest and lowest values of the parameter. Eff: Efficiency, B_L- Leakage field, Δk – variation in k due to misalignment*

(geometry and materials) in which the magnetic flux is generated or interacts with defines the IPT coupler's losses or its quality factor. Therefore, the coil designers must ensure these characteristics are met during the coupler innovation stage.

IV. Coil Design Process

The coil design is a complex process which requires identifying the objectives, constraints, limitations from power electronics system design, and EV standards such as SAE J2954 [17], IEC 61980-1:2015 [18],and ISO 19363:2020 [19], choosing correct materials, understanding on different FEA modelling methods and their tradeoffs, and thermal modelling.

A. Design Objectives

Multi-objective optimization methods based on genetic and evolutionary algorithms, and analytical methods are proposed to optimize couplers as highlighted in section III-I and Table I. Optimum coil parameters are derived by evaluating their impact on the objectives of the IPT system. The following objectives are frequently considered for optimization:

1) Transmission efficiency (η_c)

The maximum transmission efficiency of an series-series compensated IPT system can be defined in terms of the coupling coefficient (k) and quality factor of the transmitter (Q_{Tx}) and receiver (Q_{Rx}) coils, as:

$$\eta_c = \frac{k^2 Q_{Tx} Q_{Rx}}{\left(1+\sqrt{1+k^2 Q_{Tx} Q_{Rx}}\right)^2} \approx 1 - \frac{2}{kQ} \tag{1}$$

Where the quality factor $Q = \sqrt{Q_{Tx} Q_{Rx}}$ is the geometrical mean of individual quality factors. The quality factor of a coil at operating frequency (f) is given by $Q_L = \frac{2\pi f W_L}{P_L}$, where W_L is the peak energy stored in the coil, and P_L is the average power loss due to losses in shields, copper conductors, and magnetic materials. The term "figure of merit", FOM= kQ is introduced as the maximum efficiency is governed by the product of the coupling coefficient and quality factor according to (1). Equation (1) and the FOM definition is also valid for series-parallel compensated IPT system[20]. Therefore, maximizing k and Q are the key to maximize efficiency [20]. Alternate methods to evaluate the efficiency are proposed in [21],[63],[89]. The η_c is the frequently utilized objective for optimization, while *k and Q* are also considered by some designers, as shown in Table I. In the literature, a coil's misalignment tolerance (M_T) is calculated based on the difference between the maximum efficiency and efficiency during misalignment [21]. It is desirable to minimize the efficiency difference to achieve a higher misalignment tolerant coil [65].

2) Power density (α)

The power density of a coil can be interpreted in terms of the volumetric ($\alpha_V = P_o/V_c$), area ($\alpha_A = P_o/A_c$) and gravimetric ($\alpha_G = P_o/W_c$) power density [20]. V_C, A_C, and W_C are the volume, surface area, and weight of the coil. Smaller coils result in a high α_V, and α_A at the expense of higher temperatures, which require cooling systems to operate satisfactorily. Power loss density is also used as an alternative objective to the power density of the coil [86].

3) Stray magnetic field (B_{Lf})

The leakage or stray magnetic field at a point in a 3D space is given by:

$$B_{Lf} = \left(B_x^2 + B_y^2 + B_z^2\right)^{1/2} \tag{2}$$

Where B_x, B_y and, B_z are the magnetic flux density in x, y, and z-direction. Recently, proposed coil designs define an objective called power per leakage (PPL) to analyze the leakage flux generated by coils compared to their output VA rating(transferred power), and it is given by[33],[87]:

$$PPL = \frac{Output\ power}{Peak\ Leakage\ filed} \tag{3}$$

4) Cost (C_T)

The cost of an IPT coil is given by:

$$C_T = C_L l_L + C_F V_F + C_S A_S \tag{4}$$

Where C_L, C_F, and C_S are cost coefficients of Litz wire, ferrite core, and aluminum plate. l_L, V_F, and A_s are the Litz wire length, ferrite core volume, and area of the passive shield [88]. The diameter, number, and arrangement of the strands must be taken into account in determining the cost coefficient of Litz wire. The Litz wire volume can also be used instead of the length with the appropriate cost coefficient. Weight and volume are other objectives considered during coil optimization.

External factors impose limitations on the parameters and objectives of the coil design, which can be identified as constraints to the design domain. These external factors can be extracted through a detailed analysis of the PE system considered for the IPT design and also from the design guidelines provided in industrial standards such as SAE J2954/1[17], IEC 61980-1:2015, ISO 19363:2020 , and IEEE C95.1-2345-2014[27].

B. Design Constraints

1) Impact of Power Electronics Systems

In literature, most of the IPT pads are optimized for predetermined objectives, and then the PE system is designed to match the parameters of the optimized pad [28],[29]. Failure to consider the impact of the PE system parameter may result in non-optimal operation, as highlighted in [20], and [89]. There are different converter topologies [90],[91] and compensation techniques [92]-[95] that can be utilized to transmit power from the primary to the secondary pad.

Fundamentally, primary compensation minimizes the VA rating of the converter's input-side while the secondary compensation maximizes the power transfer by negating the impact of the Rx-coil's inductance[94]. The constant current or constant voltage output operations of the IPT system also depends on the selected compensation topology. Besides, compensation plays a critical role in achieving turn-on zero voltage switching (ZVS) of the converter, where the input phase

angle of the system can be modified by changing the capacitor to operate above the resonance[92]. The ZVS minimizes the switching loss of the IPT system. The input side converter of an IPT system operates on variable or constant frequency mode. The converters operating in the variable frequency mode may come across frequency bifurcation phenomenon, where multiple zero phase angles of the input impedance (Z_{in}) due to the variation from capacitive characteristics to inductive. Therefore, it is important to identify bifurcation boundaries to ensure that the controller is designed appropriately. Table IV summarizes the key advantages and disadvantages of various compensation techniques from the coil design perspective. A detailed review on compensation techniques can be found in [92][94].

The impact of compensation techniques on an IPT system can be studied by analyzing the input impedance seen by the power supply. The total impedance of a primary pad is the summation of self-impedance of the coil, impedances presented by the ferrites and conductive material of the secondary coil, and the reflected impedance caused by the windings and the tuning of the secondary pad [21]. The primary pad's inductance increases with the approach of the ferrites of the secondary pad for couplers with similar pad sizes, while it reduces with the approach of the shield of the secondary pad for mismatched size systems. These variations may have a critical impact on the limitations imposed by the PE system on coil design if not considered during the design stage. The reflected impedance varies with the compensation strategy employed. The load impedance of the secondary side (Z_s) depends on the compensation topology, and its loading effect on the primary is represented by the reflected impedance (Z_r), as shown in Fig. 6 for a series and parallel compensated primary[96]. The Z_r is

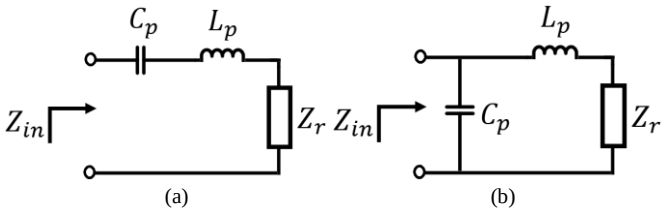

Fig. 6. Compensation topologies (a). Primary side with series compensated. (b). Primary side with parallel compensated.

given by $\frac{\omega^2 M^2}{Z_s}$. The $Z_s = j\omega L_s + \frac{1}{j\omega C_s} + R_L$ for a series compensated secondary while $Z_s = j\omega L_s + \frac{1}{j\omega C_s + \frac{1}{R_L}}$ for a parallel compensated secondary [96]. L_s and C_s are the secondary side inductance and capacitance, while R_L is the load. The reactance of Z_r is zero for a series compensated secondary while it is capacitive for a parallel compensated system [96]. It is critical to model the characteristics of the load impedance or input impedance (Z_{in}) seen by the power supply to ensure efficient power transfer and controllability. The Z_{in} of Fig. 7(a) and (b) is given by: $Z_{in} = j\omega L_p + \frac{1}{j\omega C_p} + Z_r$ for series compensated primary while $Z_s = \frac{1}{j\omega C_s + \frac{1}{j\omega L_p + Z_r}}$ for a parallel compensated primary [96]. To minimize the VA rating of the power supply, it is desirable to operate at the zero-phase angle frequency (ZPAF) of Z_{in} as the reactive power will be zero at this frequency. Therefore, the primary capacitance can be designed to compensate both the primary inductance and Z_r, as shown in [96]. The parameters of Z_{in} can be converted and normalized so that it becomes a function of operating radian frequency, coupling coefficient, primary and secondary quality

TABLE IV
ADVANTAGES AND DISADVANTAGES OF COMPENSATION NETWORKS [13],[14],[92]- [94]

Compensation	Advantages(A)/Disadvantages(D)
SS Bifurcation criteria: $Q_p > \frac{4Q_s^3}{4Q_s^2 - 1}$	A: Primary and secondary capacitance is independent of variation in coupling coefficient and the load at the resonant frequency, Higher efficiency at lower coupling coefficient, and Unity power factor at resonance, low sensitivity towards misalignment. A: Least copper usage compared to SP, PS, and PP. D: Requires an Rx-coil with higher self-inductance compared to SP. D: Undesirable operating conditions at light loads, Poor partial load efficiency due to the voltage transfer ratio's load dependency.
SP Bifurcation criteria: $Q_p > Q_s + \frac{1}{Q_s}$	A: Primary capacitance is independent of variation in the coupling coefficient and the load at the resonant frequency. A: It requires less self-inductance on the secondary side than SS topology. D: Current control is required at the primary-side independent of the loading condition and even in the absence of the receiver. D: The power factor will vary with mutual inductance. D: Primary capacitance is dependent on the coupling coefficient. Therefore, resonant frequency changes.
PS Bifurcation criteria: $Q_p > Q_s$	A: Capable of achieving higher efficiency and power factor at low mutual inductances, and during load and mutual inductance variations. D: Input must be a current source to avoid instantaneous changes in voltage. D: Primary capacitance is dependent on coupling and the load D: Higher driving voltage is required to transfer power due to relatively high input resistance.
PP Bifurcation criteria: $Q_p > Q_s + \frac{1}{Q_s}$	A: Current source behavior due to parallel compensation and favorable for battery charging applications. D: Input requires a large current source and low power factor and higher load voltage at the secondary side. D: Primary capacitance is dependent on coupling and the load.
SPS	A: Capable of maintaining constant output power under misalignments.
LCL-P	A: Improved performance against load variation. D: Increased in reactive current in the primary as the reflected impedance consists of the load's imaginary components.
LCL-S	D: The larger capacitor is required to ensure continuous conduction at the output of the rectifier. D: Increase in the output voltage with the increase in power transferred.
LCC	A: Eliminates bulkier, costly inductors of LCL. A: Capable of achieving zero current switching or zero voltage switching, independent of variations in coupling coefficient and load
LCC-LCC	A: Reduction in the current stressed of the input side converter, independent of load variation, and high misalignment tolerance

factors, and parasitic resistances of the primary and secondary coils [97].

$$Z_{in} = Z(\omega_n, k, Q_p, Q_s, R_{np}, R_{ns}) \quad (5)$$

It was observed that there are multiple ZPAF in the Z_{in} curve, depending on the primary and secondary quality factor[96]. This phenomenon is called bifurcation, and it is important to identify the boundaries of bifurcation to ensure the appropriate design of the controller. In literature, the criteria to avoid bifurcation phenomenon or realize single ZPAF are presented in terms of the quality factors of the primary and secondary side, as shown in Table IV [96]. The primary and secondary quality factors depend on the compensation techniques. For a series compensated secondary side the primary quality factor is $Q_p = \frac{L_p R_L}{\omega_0 M^2}$ while the secondary quality factor is $Q_s = \frac{\omega_0 L_s}{R_L}$. For a parallel compensated secondary, the primary quality factor is given by $Q_p = \frac{\omega_0 L_p L_s^2}{M^2 R_L}$ while secondary quality factors is $Q_s = \frac{R_L}{\omega_0 L_s}$. It is evident that for a given operating radian frequency and a rated load, the Q_p and Q_s are a function of coil parameters such as inductances and mutual inductances. Therefore, coils must be carefully designed to avoid the bifurcation phenomenon. Alternatively, Z_{in} also dependent on the coupling coefficient for a given operating radian frequency[89]. The magnitude of input impedance Z_{in}, phase angle for a SS compensation IPT system for various coupling coefficients are drawn, as shown in Fig. 7. In this paper, SS compensation topology is used to demonstrate the bifurcation phenomenon with the coupling coefficient. However, similar design thinking applies to other compensation topologies as well. The magnitude of Z_{in} and phase angle with respect to the operating frequency depends on the nominal coupling coefficient (k_0). If the coupling coefficient of the system greater than the critical coupling coefficient (k_c), there are two minima in Z_{in} and three ZPAFs, as seen in Fig. 7 (a) and (b). The critical coupling coefficient is the inverse of the external quality factor of the receiver resonant circuit. Furthermore, there are two peaks in the voltage transfer ratio (VTR) or voltage gain curve shown in Fig. 7(c). Therefore, due to bifurcation, the output voltage deviates from the initially designed values, and there is a risk of zero current switching instead of zero voltage switching of the inverter, which increases the losses. However, if k_0<k_c, there will be a single *ZPA*, minimum Z_{in}, and a single *VTR*, as shown in Fig. 7 (a), (b), and (c). Therefore, the phase angle will always be positive above the operating frequency, and ZVS can be achieved at a frequency slightly above the resonance frequency.

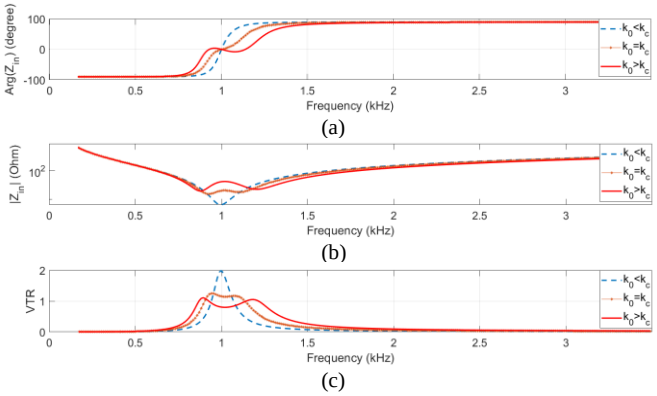

Fig. 7. (a). Phase angle of input impedance depending on k_0, (b). Magnitude of input impedance depending on k_0, (c). Voltage transfer ratio (VTR) SS compensated IPT system

Furthermore, the transmitter current's harmonics will experience larger input impedance, as seen from Fig. 7(b), which reduces their magnitude and total harmonic distortion of the transmitter current. The primary and secondary coils excitation currents are determined using the VTR, which becomes an input the numerical or analytical design domain. However, they are used for accurate estimation of the losses and leakage fields. It is important to highlight that the designers must carefully analyze the Z_{in} for other compensation techniques to arrive at suitable operating points for the IPT system.

In the literature, there are several design approaches proposed for SS compensation. In one approach, the receiver side inductance is adjusted from the designed value to meet the bifurcation criteria[20]. The maximum efficiency can only be realized if the load is optimally matched to the receiver's inductance[20]. In contrast, the authors in [89] proposed a new set of design equations, which impose limits on coupling coefficient, transmitter- and receiver-side inductances to ensure that the resulting design has the highest efficiency, low leakage field, and reduced current harmonics in the receiver and transmitter. The bifurcation criteria are met by limiting the coupling coefficient way below the critical coupling coefficient, as shown in this paper. It is shown that the design with the highest coupling coefficient has the maximum efficiency but does not ensure the lowest total harmonic distortion in the transmitter and receiver current. This is achieved at the expense of a 1% drop in power transfer efficiency [89]. Therefore, coil designs cannot ignore these limitations imposed by the power electronic system design as they are the key to ensure maximum transmission efficiency, low leakage field, low current harmonics, etc. These limitations become constraints and design inputs to the coil design stage.

2) Impact of Industrial Standards

As seen in section III of this paper, various coil designs are proposed in the literature. Therefore, it is essential to develop standards that manufacturers can follow to bring about the commercialization of IPT technology and its smooth operation. Therefore, these standards must address design considerations such as efficiency, interoperability, safety concerns, limits of various design parameters. The standards, such as SAE J2954 [17], IEC 61980-1:2015, ISO 19363:2020, aims to provide an overall view on the design considerations of an IPT system. Furthermore, J2847-6 and J2931-6 standards define the communication and signaling for wireless charging systems. Besides, IEEE C95.1-2345-2014 provides insight into physiological effects at different operating frequencies [27]. In this paper, SAE J2954 is considered to elaborate on the impact of design constraints defined in the standard on the coil design. However, the discussion can be extended to other standards as they are closely related.

The SAE J2954 standard provides design constraints such as minimum efficiency requirements, allowable ground clearance of the coupler, operating frequency range, allowable misalignments in different offset directions, electromagnetic compatibility, EMF and interoperability requirements [17].

TABLE V
J2954 SPECIFICATIONS [17]

WPT Power Classes				
Power Class	*WPT1*	*WPT2*	*WPT3*	*WPT4*
Input Power	3.7 kW	7.7 kW	11.1 kW	22 kW
Minimum efficiency (%)	>85	>85	>85	TBD
Minimum efficiency (offset) (%)	>80	>80	>80	TBD

Misalignments	
Offset direction	*Range (mm)*
Δ X /Δ Y	±75 / ± *100*
Δ Z	$(Z_n-\Delta_{low})$- $(Z_n-\Delta_{high})$
Rotation, Roll and Yaw	± 2, 2 and 10 degrees

Ground Clearance	
Z-Class	*Range (mm)*
Z1	100-150
Z2	140-210
Z3	170-250

Table V lists the minimum efficiencies at nominal and offset positions for different power classes of IPT systems along with the limits of misalignments in different directions. Efficiency limitations need to be considered during the coil design or optimization stage. Table V also shows the range of ground clearance for different classes of vehicles. Limitations on the ground clearance will limit the size of the coupler. Furthermore, variations in ground clearance will alter the coupling coefficient. These variations in coupling need to be considered during the coupler design to ensure that it does not exceed the limits of the coupling coefficient derived from the requirements of the PE system design, as detailed in section IV-B(1) and also shown in [89].

As shown in Fig. 8, electro-magnetic field (EMF) exposure to the general public is limited around the EV based on regions defined under SAE J2954. EMF exposure should be limited to a minimum of 21.2 μT in regions 2 and 3 to meet the pacemaker requirements and implanted neuro-simulators. Furthermore, these limitations should also consider the worst-case misalignment scenarios listed in Table V. The operating frequency range of an IPT system is limited to 81.38 to 90 kHz to avoid any interference with the other operating frequencies of an EV. The interoperability is another important aspect of an IPT system that needs to be considered during the design stage, as detailed in section III-I. EV manufacturers may prefer different coil structures depending on the EV's size and the complexity of the IPT system. However, in a commercial environment, IPT systems from different manufacturers should be capable of operating together. Table VI lists the interoperability requirement defined under SAE J2954 based on the power classes listed under Table V. For example; the WPT 1 system should be capable of transmitting power to coils under WPT 1 and WPT 2. The IPT system should comply with the efficiencies stated under Table V when powering WPT 1->WPT 1 category. However, SAE J2954 does not impose any limitations on efficiency when operating with a different power class such as WPT 1->WPT 2.

3) Other Constraints

Some of the other constraints are derived from the IPT pad's materials, as shown in Table I for DD and DDQ. The current density of winding (J) and core loss density (P_{cd}) of the magnetic cores is limited to ensure the coupler's thermal stability. Furthermore, the flux density (B_c) of the magnetic core is limited to avoid saturation of them. The materials must be carefully selected to improve coupler performance, as discussed in the section below.

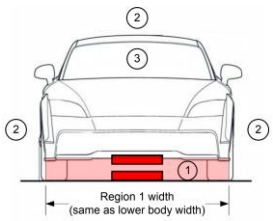

Fig. 8. EMF exposures regions to general public [17]

C. Material Selection

Materials required for coils are wires (copper tubes [98],[99], foils [100] and Litz wires [20],[101],[102]), ferromagnetic material [15],[25],[51],[52],[103],[104], passive shields [103], [104] and EMF cancel coils used for active and reactive shielding techniques [105] ,[106]. The current flowing through the copper produces the magnetic field, while ferromagnetic materials guide the field and enhance the coupling factor. Passive and active shields limit the leakage magnetic fields from the backside of the coil. These materials are selected carefully to improve the overall performance of the coupler. Optimization considers the dimensions and properties of materials to enhance the performance of the coupler [51],[52].

1) Wire/Winding

The winding is a vital component of an IPT coil as it contributes to overall performance and loss characteristics. The winding thickness must satisfy the current density limitations to ensure acceptable thermal performance [101]. Copper tubes, foils, and litz wire are used for windings [98],[100]-[102]. Litz wires are preferred over tubes due to their lower losses at higher frequencies for EV applications [20],[107]. Cable stranding, bundling, transposition, and termination are critical factors of the winding. Furthermore, the manufacturer provides guidelines in selecting a suitable Litz wire for a given application [102]. Tang et al. proposed modified copper foils as an alternative to Litz wire to further reduce the winding losses [100]. Magneto-plated aluminum pipe (MAP) with a special magnetic layer was proposed for coils to improve transmission efficiency, and reduce weight compared to solid wire, and reduce the cost compared to Litz wire. The efficiency of MAP was 1.67% lower than with Litz wire for a 3 kW system [108]. Recently, superconducting wires were introduced to reduce the coil's losses compared to Litz wires [109],[110]. However, there is no detailed comparison between the wires to conclude superiority in using superconducting material as an alternative to Litz wire.

2) Core materials

Most of the couplers proposed for EVs utilized core or magnetic materials to enhance the magnetic field. The core material is selected by considering the power rating,

TABLE VI
INTEROPERABILITY REQUIREMENTS

		Vehicle Assembly			
		WPT 1	*WPT 2*	*WPT 3*	*WPT 4*
Ground Assembly	*WPT 1*	R	R	O	O
	WPT 2	R	R	O	O
	WPT 3	O	R	R	O
	WPT 4	O	O	O	R

R- Required, O- Optional

permeability, saturation flux density, operating frequency, loss, cost, and weight. In addition, the isotropic properties of the material are also important as the spatial orientation of the magnetic field varies everywhere in the core elements, and it is a function of the positioning of the Tx and Rx coil [103]. Therefore, cores such as tape wound produce flux with spatial vector components orthogonal to the laminations. Therefore, these cores are avoided in some applications [103]. Ferrite is frequently preferred due to their lower eddy current losses compared to metallic cores, availability, higher saturation flux density, and reduced cost for EV applications [7],[20],[25],[28],[29],[50],[104]. The saturation flux density of ferrites ranges from about 370-570 mT, while their relative permeability ranges from about 1000–5000. The modern power ferrite materials can operate over 1 MHz while their heat conductivity lies in the range of (3.5 to 5.0) × 10^{-3} $Jmm^{-1}s^{-1}$ × K^{-1}. MnZn family and Nickel-Zinc family ferrites are frequently used ferrites for high power EVs and are characterized by relatively high permeability and resistivity. However, they are brittle and occupies a substantial volume inside couplers. Recently, nanocrystalline materials are proposed as a replacement for ferrite cores for IPT applications [111]. They have a higher saturation point, higher permeability, and lower coercive force compared to ferrites. However, the conductivity of these materials is higher than ferrite. Therefore, higher eddy current losses [111]. Furthermore, the amorphous material is also used in IPT applications [112]. It shows magnetic properties closer to ferrites and nanocrystalline materials but lighter in weight and fragile compared to ferrite [112].

3) Shielding materials

Active, reactive, and passive shielding techniques are utilized to shield the coupler's leakage magnetic field. Active shielding adds EMF canceling coils to both the Tx and the Rx to ensure that their corresponding canceling coil cancels the unwanted EMF from the back-side of the coil [105]. Reactive shielding techniques are introduced to eliminate additional power sources used in active techniques. Reactive shielding utilizes a passive compensation loop to generate a canceling magnetic field, which is out of phase with the leakage field generated from the IPT coupler [106]. Passive shielding techniques are frequently preferred for EVs. Core materials provide shielding for IPT couplers, depends on the shape and utilization, as discussed in section III. Conductive materials such as aluminum (Al) , OFC [103] , and copper (Cu) [113]are preferred over magnetic shielding materials due to their lower power losses [28], [103]. Losses (P_s) in the shield is given by:

$$P_s = I_e^2 R_e \alpha \sqrt{\frac{f_0}{\sigma_{sh}}} \tag{6}$$

Where, I_e, and R_e are the shield's eddy current and resistance, and f_0, and σ_{sh} are the shield's operating frequency and conductivity. According to (6), shields with high conductivity will have lower losses. Besides, field distribution in the air-gap is affected by the field cancellation due to eddy currents, resulting in a lower coupling coefficient and variations in the coil's self-inductance. Therefore, the shield should be incorporated during the design and optimization stage to avoid unexpected deviations during the hardware implementation stage.

Placement of the shield and its size, material, and thickness are critical parameters that require detailed attention. Recently, hybrid shielding structures (AL plate and Cu rings) were proposed to suppress the EMF below ICNIRP limits and reduce the shielding losses [113]. A Litz-wire based passive shielding method is proposed in [114], which can reduce the shield losses by 56% compared to the conventional Al shield.

The selected materials' properties will be used to evaluate the coil design objectives and define the constraints. Coil parameters are calculated and optimized with the aid of analytical methods [20], [115],[116] and numerical methods which include FEA tools such as JMAG, ANSYS Maxwell and, FEM, or a combination of both methods[20],[50],[117]. Challenges and limitations are unique to both approaches.

D. Modelling Methods

1) Analytical methods

Analytical methods are proposed to estimate the parameters of the coil by evaluating their design objectives. Coil losses can be estimated analytically, as discussed in [20], [115], [116]. Skin and proximity loss densities are estimated as;

$$p_{skin} = n.R_{dc}.F_R(f_0).\left(\frac{\hat{I}}{n}\right)^2 \tag{7}$$

$$p_{prox} = n.R_{dc}.G_R(f_0).\left(\hat{H}_e^2 + \frac{\hat{I}}{2\pi^2 d_a^2}\right)^2 \tag{8}$$

n and d_a are the number of strands and the outer diameter of the itz wire. F_R and G_R are frequency-dependent factors that model skin and proximity factors [118]. R_{dc} is the unit length resistance of a single strand. $\hat{I}$ is the peak current value and $\hat{H}$ is the external magnetic field penetrating the winding. The parameter $\hat{H}$ varies from one turn to another. Therefore, FEA tools are used to estimate $\hat{H}$ of an individual turn. However, this method is useful when FEA tools do not provide the loss calculation option for stranded conductors [20].

Core losses are calculated by integrating the core loss density according to the Steinmetz formula:

$$P_c = k f^{\alpha} \hat{B}^{\beta} \tag{9}$$

Where P_c is the time average loss per unit volume. k, α, and β are Steinmetz parameters for a given magnetic material and $\hat{B}$ is the peak flux density under sinusoidal excitations at resonant frequency (f). These parameters are temperature-dependent, and nominal operating temperature is considered for loss calculations. These losses can also be calculated with the aid of FEA tools by using the Steinmetz parameters of the material.

Analytical methods to estimate coil inductance [117], mutual inductance [119],[120], and efficiency [121] are also proposed. Furthermore, Kim et al. proposed an analytical method to determine the coil's number of turns based on the voltage gain, equivalent load resistance, coupling coefficient, and individual inductance of a single-turn coil [89]. Coil turns are determined to satisfy the conditions required for a low leakage magnetic field. This method does not consider the coil's losses and may not be successful for coils with complex winding structures such as DDQP, BBP, and TPP. However, with the introduction of the ferromagnetic materials, analysis based on analytical equations becomes impractical and complex due to the field-shaping. Therefore, a simulation approach based on finite

element analysis (FEA) is frequently utilized in the literature [20],[28],[37],[39],[40],[118],[122].

2) Numerical methods

Finite element analysis is a frequently used software-based method for designing coil structures due to the complexity in designs[2],[7],[20],[28],[29]. Alternative numerical methods such as integral equation (IE) formulations [123], scalar potential finite difference(SPFD) numerical scheme [124], scaled-frequency finite-difference time-domain (SF-FDTD) [125] are proposed in addition to finite element methods (FEM) to evaluate various aspects of IPT systems due to the challenges encountered with FEM. This paper discusses some of the challenges encountered with finite element analysis based modeling.

Two-dimensional (2D) [47],[54] or Three-dimensional (3D) [20],[28],[29],[42] modeling methods are used depending on the complexity of the coil structure and optimization problem formulation. 2D based coil modeling is preferred due to its simplicity and reduced computational cost compared to 3D. However, a limited number of coupler types can be modeled with 2D modeling. **Fig. 9** shows some examples of different 2D and 3D models for a CP. Cylindrical about the *z*-axis (CZ) and Cartesian *xy* (CXY) are the two major geometrical modes available to model 2D coils in ANSYS Maxwell. The CZ mode can only be used to model CP or geometries, which are cylindrical, as the design should be symmetrical about the z-axis. CP is modeled using CZ mode is shown in Fig. 9 (a) and Fig. 9 (b). Most of the coils cannot be realized with CXY mode and will not be discussed in this paper. 3D modeling can be utilized to analyze any complex coil structure shown in Fig. 4 compared to 2D modeling [20][28][29][42]. Fig. 9 (c) and Fig. 9 (d) show 3D models of the CP. However, the drawbacks in 3D modeling are the higher computational cost and the complexity in geometry realization.

The coils can also be modeled as individual turns, as shown in Fig. 9 (a), and (c). The copper turn's diameter is selected to provide the right balance between copper loss, utilization, and current density limitations to ensure acceptable thermal performance [29],[101]. They can also be modelled as a copper block, as shown in Fig. 9 (b) and (d), provided that it is excited with the appropriate current density distribution. The space between turns cannot be modelled with block-based modelling. However, block-based modeling is frequently used in the literature as it takes less time to simulate than turn-based modeling. The Litz wire with skin and the proximity effects can also be modelled at the expense of computational cost.

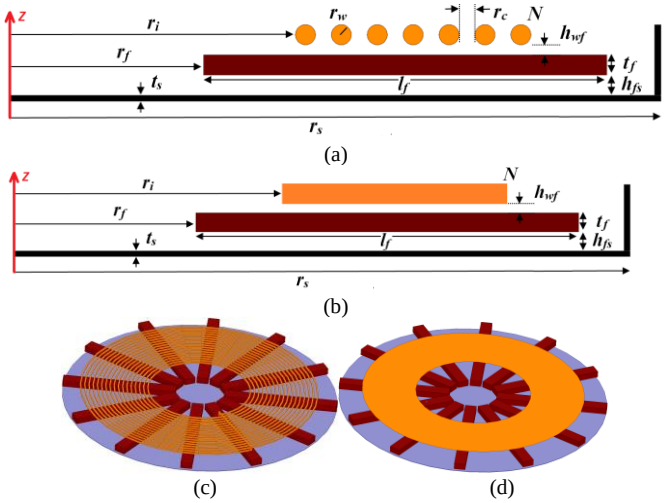

Fig. 9. 2-D and 3D modeling methods: (a) CP-turns based 2D-cylindrical about z-axis (b) CP-block based 2D-cylindrical about z-axis (c) CP-3D-turn based (d) CP-3D-block based

3) Thermal Modelling

Thermal modeling is critical since it affects the accuracy of efficiency estimation (conductivity and permeability are temperature dependent), thermal stress, power density, and safety issues [103], [85], [126]-[128]. An IPT system's losses are mainly due to the losses in Cu winding (P_{cu}), core losses in magnetic materials (P_c), and the losses in the shielding materials (P_s). These losses are a function of temperature, frequency, and material properties. These losses generate heat, which dissipates through conduction, convection, and black body radiation of electromagnetic energy. The thermal model for a typical IPT coil with ferrite bars, winding and, shielding is shown in Fig. 10. Heat conduction from the inside hotspot of the winding, core, and the shield to the surface is modelled using the thermal resistances $R_{c\text{-}s}$, $R_{f\text{-}s}$, and $R_{s\text{-}s}$ respectively, while the heat convection from the surfaces of the winding, core, and the shield to the ambient environment is modelled using the thermal resistances $R_{cs\text{-}a}$, $R_{fs\text{-}a}$, and $R_{ss\text{-}a}$, respectively[103]. The thermal models are applied to the top and bottom surface of the copper winding and the shield, as shown in Fig. 10(a) and Fig. 10(c), while the core's bottom surface is neglected due to minimal impact, as shown in Fig. 10(b) [103]. The power loss distribution is not uniform for winding, core, and the shielding and must be determined using FEA analysis. However, the uniform distribution of losses is assumed to expedite the design process[103]. The thermal resistance for a homogeneous material experiencing heat conduction in one direction is given by [127]:

$$R_{cond} = \frac{1}{k}\int \frac{dx}{A(x)} \tag{10}$$

The thermal conductivity of the material is given by *k*, while *A* is the cross-sectional area normal to the heat flow. (10) can be used to model the thermal resistances due to conduction ($R_{c\text{-}s}$, $R_{f\text{-}s}$, and $R_{s\text{-}s}$). The maximum surface-related power loss densities for the winding, core, and the shield can be calculated by using:

$$p_{Lm} = h(T_{max} - T_{amb}) \tag{11}$$

Where *h* is the heat transfer coefficient while T_{max} is the maximum allowable temperature on the surface while T_{amb} is the surrounding environment's ambient temperature [103]. (11) can be applied to determine the power loss densities

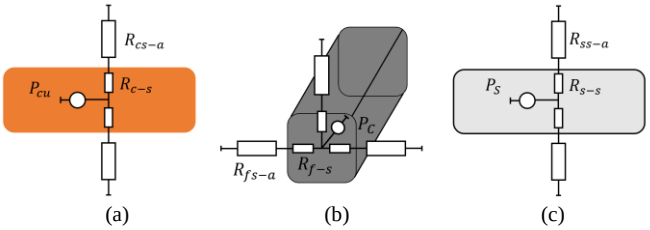

Fig. 10. Thermal Model (a). Copper winding of the magnetic pad, (b). Core of the magnetic pad, (c). Shield of the magnetic pad.

corresponding to winding, core, and the shield. Therefore, thermal resistance corresponding to convection is given by:

$$R_{conv} = \frac{1}{hA} \quad (12)$$

Heat dissipation through radiation is not analytically modeled in literature. However, it has a significant impact on the accuracy of the thermal model according to the simulation-based thermal analysis performed in [85].

Table VII summarizes recent thermal models (TM) and analyses (TA) proposed for EV application. A thermal-analytical model for a 50-kW rectangular coil structure is presented in [50][103]. The authors observed that the thermal resistances modeling conduction is significantly smaller than the convention, and it is mainly due to the Litz and ferrite's thermal conductivity. Thermal models of ferrite and the winding is incorporated into the design process with the assumption of 80 ^{0}C operating temperature, and the surface temperatures are calculated based on the power losses. A reduced-order model is introduced to facilitate faster optimization [126]. However, the model does not consider the impact of the radiation heat transfer, and it reports a 25% error compared to measured results. A Multiphysics time-dependent model is proposed to analyze the thermal behavior of a circular coil [128]. It includes a fluid dynamic model to improve the accuracy of thermal analysis during air convection. However, these models are computationally expensive to include during the optimization process. Thermal optimization of the magnetic couplers is proposed based on the mechanical structure adjustments, such as the gap between the aluminum shield and the magnetic core, and material characteristics such as modification of the aluminum shield by applying heat dissipation paint and rough processing[85]. These adjustments are made within the allowable range of the coil's electric parameters under its natural cooling condition. Therefore, strengthening heat dissipation has the potential to reduce the forced air requirements.

An accurate thermal behavior of the coupler and the surrounding area can be modeled by coupling the FEA tools with a computational fluid dynamic analysis tools [129]. However, coupled simulations are computationally expensive for use during optimization, and designers have little freedom in automating the optimization process. Coil materials are often carefully selected to satisfy the temperature performance [20],[45]. Therefore, it is important investigate further on the topic of developing analytical thermal models for IPT couplers which can be used during optimization.

V. Design Example

This paper presents a design example based on FEA analysis to highlight some research gaps and possible improvements in the coil design process. The coil structure is designed for the class of WPT 1 with a power rating of 3.7 kW and an air gap of 150 mm. The SS compensated power electronic system is considered, and the coupling coefficient is limited, as shown in section IV-B (1), to avoid bifurcation, and coil inductance is also constrained according to the design methods discussed in [89]. These constraints will limit the geometrical size of the coil during optimization. The operating frequency of 85 kHz is selected to adhere to the limits imposed by SAE J2954. The circular coupler is used for the analysis. However, the design concepts apply to other IPT pads discussed in section III. The copper for the winding, ferrite material for the core, and aluminum for the passive shield are the coil's selected materials.

The circular coils are designed using *2D* models with two modelling variations to demonstrate the impact of modelling on optimization. In design one, coils are modelled as individual turns, as shown in Fig. 9(a), while the second design's winding is modelled as a copper block, as shown in Fig. 9(b). As seen in Fig. 9(a) and (b), the parameter r_c (space between the coils) is absent in block-based modeling. Both designs use the cylindrical about the *z*-axis drawing method.

Efficiency, leakage magnetic field, area-related power density, and gravimetric power density are the optimization objectives. Multi-objective optimization based on 3D-Pareto-fronts is used to aid the selection of Pareto optimal design. The other constraints, such as operating frequency (85kHz), ground clearance(150mm), efficiency (>85%), leakage field (>21.2uT), are extracted from the SAE J2954 [17].

Table I summarizes the IPT pad designs proposed in the literature in terms of the number of design variables considered for optimization. The selected parameters vary from one solution to another. More often, design parameters are randomly selected for optimization. As a result, the proposed solutions may not be optimum and presents a weak problem formulation for the optimization algorithm. Therefore, this paper proposes a sensitivity analysis to overcome the uncertainty in selecting design parameters. It can identify and quantify the impact of individual parameters on the design objectives. Therefore, certain parameters have a higher impact on a given objective than others, and the parameters with the least impact are ignored from the optimization to reduce the computational cost and improve the overall efficiency of the optimization algorithm.

TABLE VII
COMPARISON BETWEEN THERMAL MODELS AND ANALYSIS

Ref	P (kW)	*Method*	*Conv*	*Cond*	*Rad*	*cooling*
[103]	50(TM)	*A/S*	*Yes*	*Yes*	*No*	*FA*
[126]	2(TM)	*A*	*Yes*	*Yes*	*No*	*N*
[128]	22(TM)	*S*	*Yes*	*Yes*	*No*	*FA*
[85]	NA(TA)	*S*	*Yes*	*Yes*	*Yes*	*N*

Conv- Convention, *Cond*- Conduction, *Rad*- Radiation, TM-Thermal modeling, TA- Thermal analysis A- Analytical, S- Simulations, *FA*-Forced air, *N* -Natural air

TABLE VIII
COEFFICIENT OF PROGNOSIS MATRIX

	Coil					***Block***				
	η	B_s	α_A	α_G	**k**	η	B_s	α_A	α_G	**k**
r_w	0	3.8	8	3	4.3	4.3	9.6	10	3	34
r_i	28.9	26	10	0	5.5	64	76.6	13	0	37
r_c	61.3	47	13	0	31	*NA*				
h_{wf}	0.1	0	0	0	0	0.1	0	0	0	0
r_s	3.7	1.5	15	7	3.5	11	2.7	16	7	3
t_f	0	1	0	33	1	0.7	2.3	0	33	1
r_f	0	0	22	0	0	0	0	25	0	0
t_s	0	0	0	7	0	0	0	0	7	0
l_f	4.8	10	31	50	53	19	6.6	35	50	24
h_{fs}	0.5	0.6	0	0	0.7	0.4	0.6	0	0	0.8

**Numerical figures list the percentage of importance*

Initially, a sensitivity analysis is performed using optiSLang [131]. Table VIII shows the coefficient of prognosis matrix of the parameters derived from the meta-model of the optimal prognosis approach [130],[131]. The meta-model is created with the aid of 100 design samples with the Advanced Latin Hypercube sampling approach. The percentages of importance are not similar for both methods due to the absence of r_c in blocked based modeling [131]. This clearly highlights the importance and impact of modelling method on the optimization process. Linear regression plots are used to identify the parameter's behavior towards an objective, as shown in Fig. 11. Moreover, Fig. 11 (a) shows the impact of ferrite length (l_f) on efficiency, where an increase in "l_f" tends to increase efficiency. Fig. 11 (b) shows the impact of the inner radius (r_i) on leakage field, where an increase in "r_i" tends to increase the leakage field. The parameters r_w, r_c, r_i, r_s, and l_f have the highest impact on the two main objectives, efficiency and leakage magnetic field. The design parameters such as h_{wf} and h_{fs} have a lower impact on all the objectives considered. Therefore, these parameters can be ignored during the optimization process to reduce computational cost.

Coils are optimized with the aid of particle swarm optimization (PSO) algorithm and meta-models. The block-based modeling needs fewer design simulations to derive the Pareto-front than turn-based modeling, as shown in Table IX. This is mainly due to the absence of r_c with blocked based modelling. Even though the exclusion of r_c was due to the modeling methods, it is crucial to notice the impact of number parameters on the optimization algorithm's computational time. The removal of less significant parameters via sensitivity analysis can play a significant role in reducing computational time. Table IX lists some of the best designs of both methods extracted from the 3D Pareto-fronts of the designs shown in Fig. 12. Fig. 12 (a) and (b) shows the Pareto optimum design solutions for the block-based design, while Fig. 12(c) shows all possible design solutions. Black points in Fig. 12(c) correspond to the designs that violated the constraints, while grey points are not Pareto optimum. Therefore, designs represented by black and grey points are ignored, and a Pareto-optimal solution can be selected for the implementation based on Fig. 12(a) and (b),

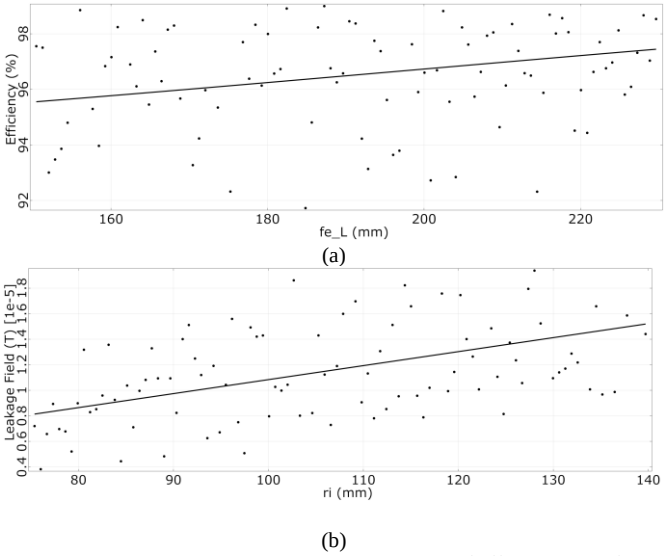

(a)

(b)

Fig. 11. Linear regression plots [131] (a). Variation of efficiency with ferrite length (b). Variation of leakage field with inner radius

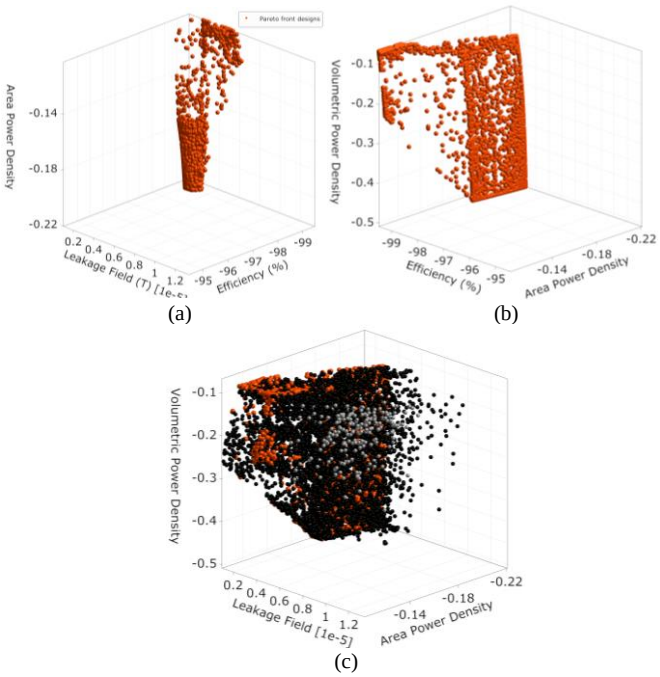

(a) (b)

(c)

Fig. 12. Pareto-fronts of the block-based coil optimization [131] (a) and (b) 3D-pareto front (c) Pareto front with invalid designs

depending on the design requirements. The reduction in efficiency and increase in leakage magnetic field is visible with the blocked based modeling. It is mainly due to the absence of r_c and higher ferrite utilization. The importance of r_c in maximizing coupling is highlighted in [47]. However, the optimization results are highly subjective to the modeling method, parameters, and optimization algorithm. Therefore, designers must carefully select these factors to improve the accuracy of the optimized coil design.

The coils are optimized at their nominal position without considering the impact of misalignments. A receiver pad can be

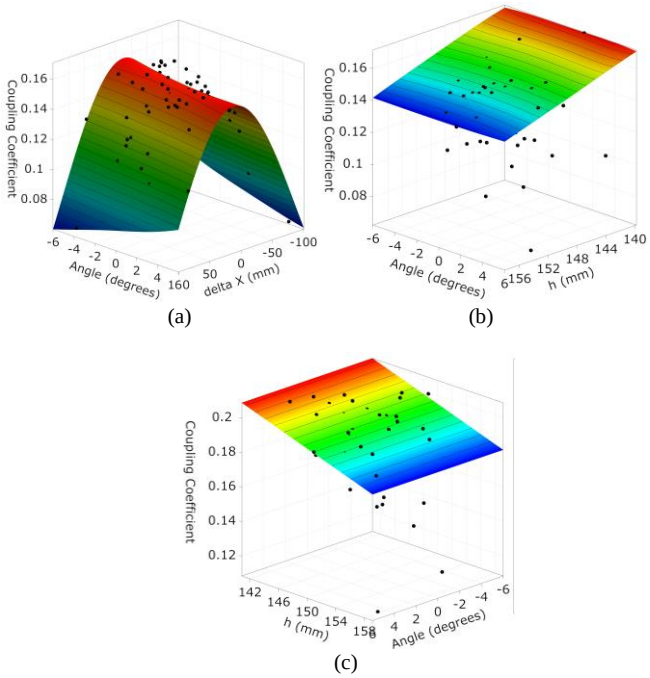

(a) (b)

(c)

Fig. 13. Variation of coupling coefficient with misalignments [131].

TABLE IX
OPTIMIZATION RESULTS WITH DIFFERENT MODELING METHODS

MM	*NS*	r_i	r_s	r_c	r_w	r_f	h_f	t_s	l_f	E_{ff}	B_s	α_A	α_G
B	178	87	69	0	2.5	65	25	1	182	94	6.3	0.15	0.33
T	200	83	68	3.3	1.9	69	25	1	150	98	2.7	0.19	0.52

MM-Modelling method, *NS- Number of simulations*, *B*- Copper block based, *T*- Copper Turns based, B_s –Leakage Field and E_{ff}- Efficiency, Units of all the parameters are in mm.

misaligned in three-dimensional space in the x-axis, y-axis, z-axis, and rotationally compared to the receiver. The selected designs from the optimal Pareto front may violate if these misalignments are considered. The variation of the coupling coefficient of the optimized coil with the misalignment is shown in Fig. 13. The black dots of Fig. 13 represent the coupling coefficient that corresponds to misalignment scenarios. Individual results are interpolated to visualize the coupling coefficient variation pattern. Fig. 13(a) illustrates the coupling coefficient's variation with angular and horizontal (*delta_X*) misalignment, while Fig. 13(b) shows the variation in coupling coefficient with ground clearance and angular misalignment. The variation in the coupling coefficient will impact the transmission efficiency of the IPT system. Therefore, efficiencies in Table IX vary when considering the overall variations in the coupling coefficient with misalignment. Therefore, the designer must integrate it into the optimization to achieve an efficient design under misalignments[65].

Similarly, the variation in the coupling coefficient under misalignment may violate some of the design constraints considered during the PE system, as detailed in [89]. Fig. 13(c) shows the coupling coefficient's variation with ground clearance and angular misalignment for another optimal design chosen from the Pareto front of the optimization. The coupling coefficient is restricted to 0.19 in this design according to the guideline presented in [89] to ensure low current harmonics in the receiver and transmitter current while ensuring the maximum efficiency and minimum leakage magnetic field. However, as seen in Fig. 13(c), the coupling coefficient exceeds such limits and may result in non-optimum operation.

EMF exposure is often considered as a design objective in many optimized solutions presented in the literature [20],[50]. Alternatively, it is used as a constraint [88]. To avoid any conflicts in selecting EMF exposure as an objective or constraint, this paper proposes considering EMF exposure as an objective and minimizing its value while adhering to the limit defined under SAE J2954. Fig. 14 shows the probability density function (PDF) of the EMF exposure of an optimized design with misalignment. The interval limit shows the maximum EMF exposure limit defined under SAE J2954 (21.2 µT). The EMF exposure is measured at 650 mm from the center of the coupler fixed to a 1.7 m wide-vehicle shown in Fig. 8. As seen in Fig. 14, the design is well below the maximum allowable limit specified under SAE J2954. As seen in Fig. 12 (a) and (b), numerous solutions are available that satisfy the initial design requirements. However, they may not be optimum when considering factors such as misalignment. Therefore, the designer must carefully choose the appropriate design through an in-depth analysis or incorporate misalignment into the optimization algorithm [65].

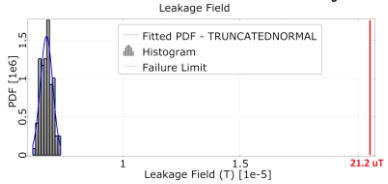

Fig. 14. Probability density function of leakage field

Fig. 15 shows the proposed universal design guideline based on the analysis and design example presented in this paper. Initially, system specifications are identified based on the requirements of the application and from industrial standards. An appropriate coil geometry is selected based on system

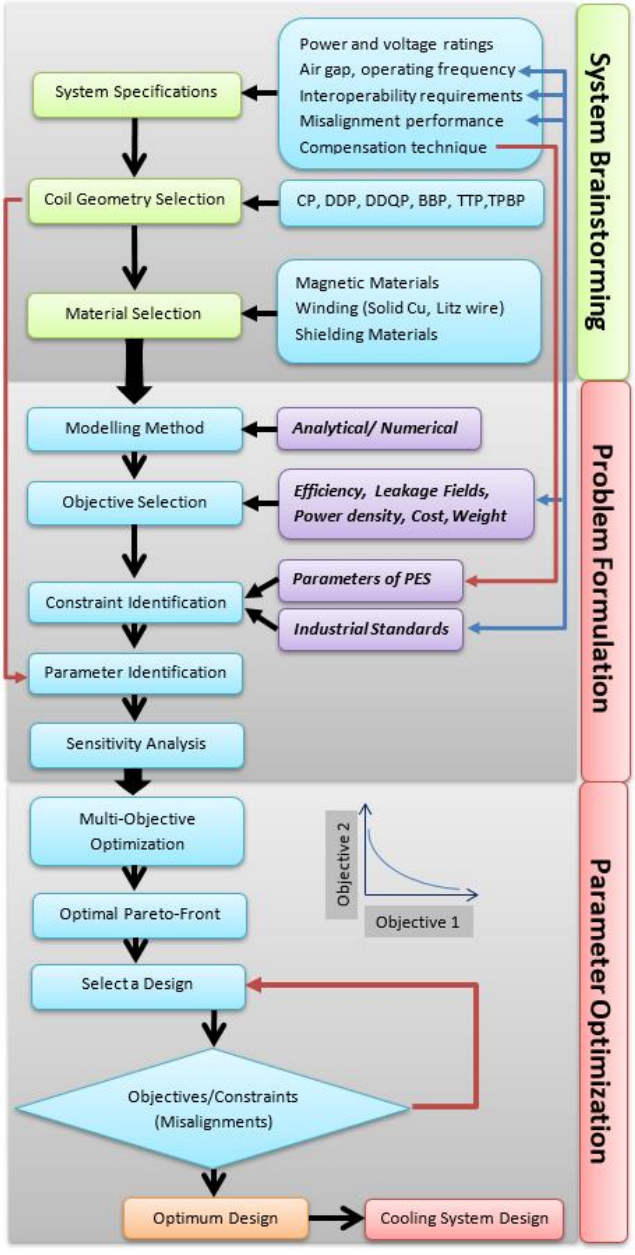

Fig. 15. Coil design guideline

specification by considering the pros and cons of different geometries, as discussed in section III. The IPT pad's material are selected based on their properties, such as low losses, cost, weight, as discussed in section IV-C. These three stages are crucial for the overall success in achieving a high performing coupler and can be identified as the "system brainstorming".

The problem formulation stage is critical, as the optimization results vary depending on the decisions made at this stage. The details of objectives, and constraint identification and modelling method selection are provided in section IV-A, B, and D. The parameters are identified based on the selected coil geometry. However, the sensitivity analysis will determine their impact on the selected objectives and avoid the least important parameters from the optimization to reduce the computational time. This will be advantageous with 3D simulations, which are computationally expensive. The multi-objective optimization is frequently preferred due to multiple objectives in designing couplers and the optimization algorithm must be selected carefully to reduce the computation cost. The Pareto optimal front is constructed from the optimized solutions. These are designs that none of the objectives can be improved without degrading the other objectives. The optimization is carried out at a nominal position without considering the impact of misalignments. Therefore, these Pareto-optimal designs may not be optimum when considering the variations in misalignments, as shown in the analysis presented in section V. Therefore, the selected design must be evaluated to ensure that it performs optimally under these variations. Alternatively, misalignments can be incorporated into the optimization loop to maximize optimization objectives while fulfilling the constraints under misalignments. The cooling system can be designed after the optimization, or thermal design can be incorporated into the optimization loop, as discussed in section IV-D (3).

VI. Future Directions

The following areas of improvements are proposed based on the review and analysis presented in this paper.

1) Coupler vs. Power Electronics

The polarized couplers such as DDQP, BBP, and TPP achieve superior interoperability performance at the expense of complex power electronics (PE) and control systems, as discussed in section III. The couplers are developed to improve misalignment and interoperability performance, and little emphasis is given to reduce the PE system's complexity, which is equally important in realizing a compact IPT system. Therefore, the designers are encouraged to explore coupler design with the consideration of PE systems.

2) Coupler vs. Misalignment Performance

There are numerous efforts to improve couplers' lateral misalignment performance through understanding the impact of parameters, as discussed in Section III. The couplers such as circular, DDP, DDQP, and BPP have poor rotational misalignment performance while TPP shows enhanced performance. However, the designers are encouraged to study the impact of various coil parameters on enhancing rotational misalignment performance as there is little research on rotational misalignments.

3) Reliability and weight

Ferrite is a brittle material that reduces IPT couplers' reliability, and these couplers undergo mechanical stress during operation. The performance aspects of complex couplers discussed in section III do not involve any reliability study, and there is a possibility for them to fail under harsh environments. Therefore, it is important to conduct a reliability study on these couplers.

Recently, a ferrite-less circular coupler called CNFP [87] and a double DD coupler [132] were proposed for EVs to improve robustness and reliability. These couplers have low coupling coefficients but high enough to maintain efficient power transfer at the expense of a higher VA rating. Field cancellation coil or reflection winding is utilized to limit the leakage magnetic field to the ICNIRP limit. The reflection winding must be appropriately designed with the least effect on the coupling. There is hardly any research on misalignment performance and interoperability of these couplers. Therefore, designers are encouraged to address these issues and provide a comparative analysis on full ferrite and ferrite-less couplers.

4) Robust coil shapes

Most of the coupler proposed in the literature are developed with conventional parametric design techniques. Topology optimization enables designers to develop new shapes compared to conventional techniques [133]. The circular coupler is optimized with the topology optimization method in [134], and the design was able to achieve a coupling coefficient of 4.1% higher at 160 mm lateral misalignment compared to the conventional circular coil [28]. The resulting shape of the ferrite core with topology optimization is entirely different from that of the conventional design shown in Fig. 4(a) and (b). Topology optimization can be extended to improve existing couplers' performance, reduce the weight and volume, and, most importantly, innovate new shapes by incorporating deep learning artificial neural networks, as shown in [135] for rotating machines.

5) Development of hybrid couplers

Recently, hybrid couplers were proposed which utilize the IPT and capacitive power transfer technologies for EVs [16],[136],[137]. The system proposed in [136] was able to transfer 2.84 kW power at an efficiency of 94.5% while [137] was able to transfer 1.1 kW at 91.9%. These hybrid couplers have the potential to improve power transfer density, misalignment performance, and reduce the compensation components [16]. However, the systems presented in the literature do not comply with the requirements of SAE J2954/1 standard such as operating frequency. Therefore, designers are encouraged to design hybrid couplers that adhere to EV standards.

6) Thermal modelling

There is a need for developing accurate analytical thermal models for high power IPT couplers that can be used during the optimization. The proposed analytical methods hardly consider the impact of thermal radiation, and it plays a vital role, as shown in [85].

7) Hybrid optimization methods

Multi-objective optimization of complex coil structures using 3D modeling is almost impossible due to the requirement of a significant number of FEA designs by optimization algorithms. However, multi-objective optimization based on the Taguchi method (TM) is proposed for electric machines in

[138], to reduce the FEA designs. Therefore, a complex IPT coil structure can also be optimized using TM and similar methods. Furthermore, sensitivity analysis can be used to reduce the number of parameters during the optimization.

8) Robust optimization

Couplers must be robust against the various combinations of misalignments discussed in section III. As shown in [134], the coupling coefficient during misalignment can be improved during optimization. Therefore, misalignments must be included in the optimization algorithms, and the impact of the coil parameters on the misalignment must be explored.

VII. Conclusion

This paper reviewed the state-of-the-art couplers and their design and optimization methodologies for stationary wireless electric vehicle (EV) charging systems. Recently proposed coil structures can achieve superior performance in coupling coefficients, efficiency, interoperability, misalignment performance, and reduced leakage magnetic flux at the expense of control and power electronics (PE) system complexity. Design methodologies are mainly based on finite element analysis (FEA) tools, and multiple objectives are considered. Therefore, multi-objective optimization strategies are proposed to improve the performance of the couplers further. Based on the analysis presented in this paper, the importance of conducting sensitivity analysis, including constraints extracted from the PE system and EV standards, and ensuring optimum design with misalignments are proposed. The impact of different modeling techniques on optimization is highlighted. Design aspects, such as thermal modeling and material selections, are also discussed. A generalized design guideline for IPT couplers is proposed based on the detailed analysis. Several future approaches are presented for IPT coupler designing.

References

[1] Y. Dingyi, W. Haiyan and Y. Kaiming, "State-of-the-art and trends of autonomous driving technology," *IEEE Int. Symp. Innov. and Entrep.* (TEMS-ISIE), Beijing, 2018, pp. 1-8.

[2] R. Bosshard and J. W. Kolar, "Inductive power transfer for electric vehicle charging: Technical challenges and tradeoffs," *IEEE Power Electron. Mag.*, vol. 3, no. 3, pp. 22-30, Sept. 2016.

[3] J. T. Boys, G. A. Covic, and A. W. Green, "Stability and control of inductively coupled power transfer systems," *IEE Proc. Electr. Power Appl.*, vol. 147, no. 1, pp. 37–43, Jan. 2000.

[4] Engineering Department at Systems Control Technology, D. M. Empey, E. H. Lechner, G. Wyess, M. Vincent, J. Garbarino, R. Moore, G. J. Bailie, J. V. Josselyn, J. Frenster, C. R. Klein, S. E. Shladover, and E. H. Lechner, "Roadway powered electric vehicle project track construction and testing program phase 3D," *Systems Control Technology Inc.*, Palo Alto, CA, USA, Tech. Rep. UCB-ITS-PRR-94-07, Mar. 1994.

[5] V. Cirimele, M. Diana, F. Freschi and M. Mitolo, "Inductive Power Transfer for Automotive Applications: State-of-the-Art and Future Trends," *IEEE Trans. Ind. Appl.*, vol. 54, no. 5, pp. 4069-4079, Sept.-Oct. 2018.

[6] G. A. Covic and J. T. Boys, "Inductive power transfer," *Proc. IEEE*, vol. 101, no. 6, pp. 1276–1289, Jun. 2013.

[7] G. A. Covic and J. T. Boys, "Modern Trends in Inductive Power Transfer for Transportation Applications," *IEEE J. Emerg. Sel. Topics Power Electron.*, vol. 1, no. 1, pp. 28-41, March 2013.

[8] S. Lukic and Z. Pantic, "Cutting the Cord: Static and Dynamic Inductive Wireless Charging of Electric Vehicles," *IEEE Electrific. Mag.*, vol. 1, no. 1, pp. 57-64, Sept. 2013.

[9] F. Musavi, W. Eberle, "Overview of wireless power transfer technologies for electric vehicle battery charging", *IET Power Electron.*, vol. 7, no. 1, pp. 60-66, Jan. 2014.

[10] S. Li, C. C. Mi, "Wireless power transfer for electric vehicle applications", *IEEE J. Emerg. Sel. Topics Power Electron.*, vol. 3, no. 1, pp. 4-17, Mar. 2015.

[11] S. Y. Choi, B. W. Gu, S. Y. Jeong, C. T. Rim, "Advances in wireless power transfer systems for roadway-powered electric vehicles", *IEEE J. Emerg. Sel. Topics Power Electron.*, vol. 3, no. 1, pp. 18-36, Mar. 2015.

[12] C. C. Mi, G. Buja, S. Y. Choi, C. T. Rim, "Modern advances in wireless power transfer systems for roadway powered electric vehicles", *IEEE Trans. Ind. Electron.*, vol. 63, no. 10, pp. 6533-6545, Oct. 2016.

[13] D. Patil, M. K. McDonough, J. M. Miller, B. Fahimi and P. T. Balsara, "Wireless Power Transfer for Vehicular Applications: Overview and Challenges," *IEEE Trans. Transport. Electrific.*, vol. 4, no. 1, pp. 3-37, March 2018.

[14] A. Ahmad, M. S. Alam and R. Chabaan, "A Comprehensive Review of Wireless Charging Technologies for Electric Vehicles," *IEEE Trans. Transport. Electrific.*, vol. 4, no. 1, pp. 38-63, March 2018.

[15] O. C. Onar, M. Chinthavali, S. L. Campbell, L. E. Seiber and C. P. White, "Vehicular Integration of Wireless Power Transfer Systems and Hardware Interoperability Case Studies," *IEEE Trans. Ind. Appl.*, vol. 55, no. 5, pp. 5223-5234, Sept.-Oct. 2019.

[16] D. Vincent, P. S. Huynh, N. A. Azeez, L. Patnaik and S. S. Williamson, "Evolution of Hybrid Inductive and Capacitive AC Links for Wireless EV Charging -A Comparative Overview," *IEEE Trans. Transport. Electrific.*, vol. 5, no. 4, pp. 1060-1077, Dec. 2019.

[17] Wireless charging of electric and plug-in hybrid vehicles, Society of Automotive Engineers, SAE Std. J2954 [Online]. Available: http://standards.sae.org/wip/j2954/. [Accessed: Sept. 20, 2016].

[18] IEC 61980-1:2015: Electric vehicle wireless power transfer (WPT) systems - Part 1: General requirements [Online]. Available: https://webstore.iec.ch/publication/22951

[19] ISO 19363:2020: Electrically propelled road vehicles — Magnetic field wireless power transfer — Safety and interoperability requirements [Online]. Available: https://www.iso.org/obp/ui/#iso:std:iso:19363:ed-1:v1:en

[20] R. Bosshard, J. W. Kolar, J. Mühlethaler, I. Stevanović, B. Wunsch, F. Canales, " Modeling and \$eta \$ - \$alpha \$ -Pareto optimization of inductive power transfer coils for electric vehicles ", *IEEE J. Emerg. Sel. Topics Power Electron.*, vol. 3, no. 1, pp. 50-64, Mar. 2015.

[21] F. Y. Lin, G. A. Covic and J. T. Boys, "Evaluation of Magnetic Pad Sizes and Topologies for Electric Vehicle Charging," *IEEE Trans. Power Electron.*, vol. 30, no. 11, pp. 6391-6407, Nov. 2015.

[22] D. V. Otto, "Power supply equipment for electrically-driven vehicle," JP Patent 49 063 111, Jun. 19, 1974.

[23] R. Laouamer, M. Brunello, J. P. Ferrieux, O. Normand, N. Buchheit, "A multi-resonant converter for non-contact charging with electromagnetic coupling", in *Proc. 23rd Int. Conf. Ind. Electron. Control Instrum.* 1997, vol. 2, pp. 792-797.

[24] H. Sakamoto, K. Harada, S. Washimiya, K. Takehara, Y. Matsuo and F. Nakao, "Large air-gap coupler for inductive charger [for electric vehicles]," *IEEE Trans. Magn.*, vol. 35, no. 5, pp. 3526-3528, Sept. 1999.

[25] F. Nakao, Y. Matsuo, M. Kitaoka and H. Sakamoto, "Ferrite core couplers for inductive chargers," " in *Proc. Power Conv. Conf*, Osaka, 2002, pp. 850-854 vol.2.

[26] R. Mecke and C. Rathge, "High frequency resonant inverter for contactless energy transmission over large air-gap," in *Proc. 35th Annu. Power Electron. Specialist Conf., Aachen, Germany*, 2004, pp. 1737–1743.

[27] IEEE standard for Safety Levels With Respect to Human Exposure to Radio Frequency Electromagnetic Fields 3 kHz to 300 GHz, IEEE, IEEE Std. C96.1–2005, Apr. 2006.

[28] M. Budhia, G. A. Covic, J. T. Boys, "Design and optimization of circular magnetic structures for lumped inductive power transfer systems", *IEEE Trans. Power Electron.*, vol. 26, no. 11, pp. 3096-3108, Nov. 2011.

[29] M. Budhia, J. T. Boys, G. A. Covic, C.-Y. Huang, "Development of a single-sided flux magnetic coupler for electric vehicle IPT charging systems", *IEEE Trans. Ind. Electron.*, vol. 60, no. 1, pp. 318-328, Jan. 2013.

[30] A. Zaheer, M. Budhia, D. Kacprzak and G. A. Covic, "Magnetic design of a 300 W under-floor contactless Power Transfer system," in *Proc. 37th Annu. Conf. Ind. Electron. Conf. (IECON)*, Melbourne, VIC, 2011, pp. 1408-1413.

[31] G. A. Covic, M. L. G. Kissin, D. Kacprzak, N. Clausen and H. Hao, "A bipolar primary pad topology for EV stationary charging and highway power by inductive coupling," in *Proc. IEEE Energy Convers. Congr. Expo. (ECCE)*, Phoenix, AZ, 2011, pp. 1832-1838.

[32] A. Zaheer, G. A. Covic and D. Kacprzak, "A Bipolar Pad in a 10-kHz 300-W Distributed IPT System for AGV Applications," *IEEE Trans. Ind. Electron.*, vol. 61, no. 7, pp. 3288-3301, July 2014.

[33] S. Kim, G. A. Covic and J. T. Boys, "Tripolar Pad for Inductive Power Transfer Systems for EV Charging," *IEEE Trans. Power Electron.*, vol. 32, no. 7, pp. 5045-5057, July 2017.

[34] Seho Kim, Grant A. Covic, John T. Boys, "Comparison of Tripolar and Circular Pads for IPT Charging Systems", *IEEE Trans. Power Electron.*, vol. 33, no. 7, pp. 6093-6103, 2018.

[35] S. Kim, A. Zaheer, G. Covic and J. Boys, "Tripolar pad for inductive power transfer systems," in *Proc. 40th Annu. Conf. Ind. Electron. Conf. (IECON)*, Dallas, TX, 2014, pp. 3066-3072.

[36] A. Tejeda, S. Kim, F. Y. Lin, G. A. Covic and J. T. Boys, "A Hybrid Solenoid Coupler for Wireless Charging Applications," *IEEE Trans. Power Electron*., vol. 34, no. 6, pp. 5632-5645, June 2019.

[37] P. Ning, O. Onar and J. Miller, "Genetic algorithm based coil system optimization for wireless power charging of electric vehicles," in *Proc. IEEE Transp. Electrific. Conf. Expo (ITEC)*, Detroit, MI, 2013, pp. 1-5.

[38] N. Hasan, T. Yilmaz, R. Zane and Z. Pantic, "Multi-objective particle swarm optimization applied to the design of Wireless Power Transfer systems," in *Proc. IEEE Wireless Power Transf. Conf. (WPTC)*, CO, 2015, pp. 1-4.

[39] T. Yilmaz, N. Hasan, R. Zane and Z. Pantic, "Multi-Objective Optimization of Circular Magnetic Couplers for Wireless Power Transfer Applications," *IEEE Trans. Magn.*, vol. 53, no. 8, pp. 1-12, Aug. 2017.

[40] A. Desmoort, Z. De Grève and O. Deblecker, "Multiobjective optimal design of wireless power transfer devices using a Genetic Algorithm and accurate analytical formulae," in *Proc. 42nd Annu. Conf. Ind. Electron. Conf. (IECON)*, Florence, 2016, pp. 4518-4522.

[41] M. Kiani and M. Ghovanloo, "A Figure-of-Merit for Designing High-Performance Inductive Power Transmission Links," *IEEE Trans. Ind. Electron.*, vol. 60, no. 11, pp. 5292-5305, Nov. 2013.

[42] S. Bandyopadhyay, V. Prasanth, P. Bauer and J. A. Ferreira, "Multi-objective optimisation of a 1-kW wireless IPT systems for charging of electric vehicles," in *Proc. IEEE Transp. Electrific. Conf. Expo (ITEC)*, Dearborn, MI, 2016, pp. 1-7.

[43] J. P. K. Sampath, A. Alphones and D. M. Vilathgamuwa, "Figure of Merit for the Optimization of Wireless Power Transfer System Against Misalignment Tolerance," *IEEE Trans. Power Electron.*, vol. 32, no. 6, pp. 4359-4369, June 2017.

[44] Y. Liu, R. Mai, D. Liu, Y. Li and Z. He, "Efficiency Optimization for Wireless Dynamic Charging System With Overlapped DD Coil Arrays," *IEEE Trans. Power Electron.*, vol. 33, no. 4, pp. 2832-2846, April 2018.

[45] R. Bosshard, U. Iruretagoyena and J. W. Kolar, "Comprehensive Evaluation of Rectangular and Double-D Coil Geometry for 50 kW/85 kHz IPT System," *IEEE J. Emerg. Sel. Topics Power Electron*, vol. 4, no. 4, pp. 1406-1415, Dec. 2016.

[46] H. Li, K. Wang, L. Huang, J. Li and X. Yang, "Coil structure optimization method for improving coupling coefficient of wireless power transfer," in *Proc. IEEE Appl. Power Electron. Conf. Expo. (APEC)*, Charlotte, NC, 2015, pp. 2518-2521.

[47] A. A. S. Mohamed, S. An and O. Mohammed, "Coil Design Optimization of Power Pad in IPT System for Electric Vehicle Applications," *IEEE Trans. Magn.*, vol. 54, no. 4, pp. 1-5, April 2018.

[48] A. Hariri, A. Elsayed and O. A. Mohammed, "An Integrated Characterization Model and Multiobjective Optimization for the Design of an EV Charger's Circular Wireless Power Transfer Pads," *IEEE Trans. Magn.*, vol. 53, no. 6, pp. 1-4, June 2017.

[49] I. U. Castillo-Zamora, P. S. Huynh, D. Vincent, F. J. Perez-Pinal, M. A. Rodriguez-Licea and S. Williamson, "Hexagonal Geometry Coil for a WPT High Power Fast Charging Application," *IEEE Trans. Transport. Electrific.*, vol. 5, no. 4, pp. 946-956, Dec. 2019.

[50] R. Bosshard, J. W. Kolar, "Multi-objective optimization of 50 kW/85 kHz IPT system for public transport", *IEEE J. Emerg. Sel. Topics Power Electron.*, vol. 4, no. 4, pp. 1370-1382, Dec. 2016.

[51] T. Shijo, K. Ogawa and S. Obayashi, "Optimization of thickness and shape of core block in resonator for 7 kW-class wireless power transfer system for PHEV/EV charging," in *Proc. IEEE Energy Convers. Congr. Expo. (ECCE)*, Montreal, QC, 2015, pp. 3099-3102.

[52] M. Mohammad and S. Choi, "Optimization of ferrite core to reduce the core loss in double-D pad of wireless charging system for electric vehicles," in *Proc. IEEE Appl. Power Electron. Conf. Expo. (APEC)*, San Antonio, TX, 2018, pp. 1350-1356.

[53] M. Mohammad, S. Choi and M. Elbuluk, "Loss Minimization Design of Ferrite Core in a DD Coil based High-Power Wireless Charging System for Electrical Vehicle Application," *IEEE Trans. Transport. Electrific.*, vol. 5, no. 4, pp. 957-967, Dec. 2019.

[54] S. Cruciani, T. Campi, M. Feliziani and F. Maradei, "Optimum coil configuration of wireless power transfer system in presence of shields," in *Proc. IEEE Int. Symp. Electromagn. Compat.*, Dresden, 2015, pp. 720-725.

[55] S. Jayalath and A. Khan, "Analysis of the Relationship between the Parameters of IPT Transformer and Power Electronic System," *Proc. IEEE Wireless Power Transf. Conf. (WPTC)*, Qubec, Canada, 2017, pp. 1-4.

[56] M. Lu and K. D. T. Ngo, "Pareto fronts for coils' efficiency versus stray magnetic field in inductive power transfer," in *Proc. IEEE PELS Workshop Emerg. Technol. Wireless Power (WoW)*, Knoxville, TN, 2016, pp. 140-144.

[57] I. Lee, N. Kim, I. Cho and I. Hong, "Design of a Patterned Soft Magnetic Structure to Reduce Magnetic Flux Leakage of Magnetic Induction Wireless Power Transfer Systems," *IEEE Trans. Electromagn. Compat.*, vol. 59, no. 6, pp. 1856-1863, Dec. 2017.

[58] M. Mohammad, S. Choi, Z. Islam, S. Kwak and J. Baek, "Core Design and Optimization for Better Misalignment Tolerance and Higher Range of Wireless Charging of PHEV," *IEEE Trans. Transport. Electrific.*, vol. 3, no. 2, pp. 445-453, June 2017.

[59] A. Moradi, F. Tahami and A. Poorfakhraei, "Minimum weight wireless power transfer coil design," in *Proc. 2016 7th Power Electron. Drive Syst. Technol. Conf.*, Tehran, 2016, pp. 571-576.

[60] J. M. Miller and A. Daga, "Elements of Wireless Power Transfer Essential to High Power Charging of Heavy Duty Vehicles," *IEEE Trans. Transport. Electrific.*, vol. 1, no. 1, pp. 26-39, June 2015.

[61] Kunwar Aditya, Vijay K. Sood, Sheldon S. Williamson, "Magnetic Characterization of Unsymmetrical Coil Pairs Using Archimedean Spirals for Wider Misalignment Tolerance in IPT Systems", *IEEE Trans. Transport. Electrific.*, vol. 3, no. 2, pp. 454-463, 2017.

[62] J. Zhang, X. Yuan, C. Wang, Y. He, "Comparative analysis of two-coil and three-coil structures for wireless power transfer", *IEEE Trans. Power Electron.*, vol. 32, no. 1, pp. 341-352, Jan. 2017.

[63] M. Lu and K. D. T. Ngo, "A Fast Method to Optimize Efficiency and Stray Magnetic Field for Inductive-Power-Transfer Coils Using Lumped-Loops Model," *IEEE Trans. Power Electron.*, vol. 33, no. 4, pp. 3065-3075, April 2018.

[64] T. Diekhans and R. W. De Doncker, "A Dual-Side Controlled Inductive Power Transfer System Optimized for Large Coupling Factor Variations and Partial Load," *IEEE Trans. Power Electron.*, vol. 30, no. 11, pp. 6320-6328, Nov. 2015.

[65] S. Bandyopadhyay, P. Venugopal, J. Dong and P. Bauer, "Comparison of Magnetic Couplers for IPT-Based EV Charging Using Multi-Objective Optimization," *IEEE Trans. Veh. Technol.*, vol. 68, no. 6, pp. 5416-5429, June 2019.

[66] N. Liu and T. G. Habetler, "Design of a Universal Inductive Charger for Multiple Electric Vehicle Models," *IEEE Trans. Power Electron.*, vol. 30, no. 11, pp. 6378-6390, Nov. 2015.

[67] H. Movagharnejad and A. Mertens, "Design optimization of various contactless power transformer topologies for wireless charging of electric vehicles," *in Proc. Eur. Conf. Power Electron. Appl*., 2016, pp. 1–10.

[68] M. Budhia, G. A. Covic, and J. T. Boys, "A new IPT magnetic coupler for electric vehicle charging systems," in *Proc. 36th Annu. Conf. IEEE Ind. Electron. Soc. (IECON)*, Glendale, AZ, USA, Nov. 2010, pp. 2487–2492.

[69] J. Deng, J. Deng, W. Li, S. Li, C. Mi, "Magnetic integration of LCC compensated resonant converter for inductive power transfer applications", in *Proc. IEEE Energy Convers. Congr. Expo. (ECCE)*, pp. 660-667, Sep. 2014.

[70] A. Zaheer, H. Hao, G. A. Covic and D. Kacprzak, "Investigation of Multiple Decoupled Coil Primary Pad Topologies in Lumped IPT Systems for Interoperable Electric Vehicle Charging," *IEEE Trans. Power Electron.*, vol. 30, no. 4, pp. 1937-1955, April 2015.

[71] F. Y. Lin, A. Zaheer,M. Budhia, and G. A. Covic, "Reducing leakage flux in IPT systems by modifying pad ferrite structures," *in Proc. IEEE Energy Convers. Congr. Expo*., Sep. 2014, pp. 1770–1777.

[72] K. Song et al., "Design of DD coil with high misalignment tolerance and low EMF emissions for wireless electric vehicle charging systems," *IEEE Trans. Power Electron*., vol. 35, no. 9, pp. 9034–9045, Sep. 2020.

[73] D. Kraus and H. Herzog, "Magnetic Design of a Q-Coil for a 10 kW DDQ System for Inductive Power Transfer," in *Proc. IEEE PELS Workshop Emerg. Technol. Wireless Power (WoW)*, London, United Kingdom, 2019, pp. 140-143.

[74] N. Rasekh, J. Kavianpour and M. Mirsalim, "A Novel Integration Method for a Bipolar Receiver Pad Using LCC Compensation Topology for Wireless Power Transfer," *IEEE Trans. Veh. Technol.*, vol. 67, no. 8, pp. 7419-7428, Aug. 2018.

[75] T. Nguyen, S. Li, W. Li and C. C. Mi, "Feasibility study on bipolar pads for efficient wireless power chargers," in *Proc. IEEE Appl. Power Electron. Conf. Expo. (APEC)*, Fort Worth, TX, 2014, pp. 1676-1682.

[76] H. Matsumoto, Y. Neba, H. Iura, D. Tsutsumi, K. Ishizaka and R. Itoh, "Trifoliate Three-Phase Contactless Power Transformer in Case of Winding-Alignment," *IEEE Trans. Ind. Electron.*, vol. 61, no. 1, pp. 53-62, Jan. 2014.

[77] F. Turki, M. Detweiler, V. Reising, "Performance of wireless charging system based on quadrupole coil geometry with different resonance topology approaches", in *Proc. IEEE PELS Workshop Emerg. Technol. Wireless Power*, pp. 104-109, Oct 2016.

[78] S.Y. Jeong, S.Y. Choi, M.R. Sonapreetha, C.T. Rim, "DQ-quadrature power supply coil sets with large tolerances for wireless stationary ev chargers", in *Proc. IEEE PELS Workshop Emerg. Technol. Wireless Power*, pp. 1-6, June 2015.

[79] F. Lin, G. A. Covic and J. T. Boys, "A Comparison of Multi-Coil Pads in IPT systems for EV Charging," in *Proc. IEEE Energy Convers. Congr. Expo. (ECCE)*, Portland, OR, 2018, pp. 105-112.

[80] A. Ahmad, M. S. Alam and A. A. S. Mohamed, "Design and Interoperability Analysis of Quadruple Pad Structure for Electric Vehicle Wireless Charging Application," *IEEE Trans. Transport. Electrific.*, vol. 5, no. 4, pp. 934-945, Dec. 2019.

[81] Y. Chen, R. Mai, Y. Zhang, M. Li and Z. He, "Improving Misalignment Tolerance for IPT System Using a Third-Coil," *IEEE Trans. Power Electron.*, vol. 34, no. 4, pp. 3009-3013, April 2019.

[82] S. Moon, B.-C. Kim, S.-Y. Cho, C.-H. Ahn, G.-W. Moon, "Analysis and design of a wireless power transfer system with an intermediate coil for high efficiency", *IEEE Trans. Ind. Electron.*, vol. 61, no. 11, pp. 5861-5870, Nov. 2014.

[83] S. Moon, G.-W. Moon, "Wireless power transfer system with an asymmetric four-coil resonator for electric vehicle battery chargers", *IEEE Trans. Power Electron.*, vol. 31, no. 10, pp. 6844-6854, Oct. 2016.

[84] J. Pries, V. P. N. Galigekere, O. C. Onar and G. Su, "A 50-kW Three-Phase Wireless Power Transfer System Using Bipolar Windings and Series Resonant Networks for Rotating Magnetic Fields," *IEEE Trans. Power Electron.*, vol. 35, no. 5, pp. 4500-4517, May 2020.

[85] C. Zhu et al., "Thermal Simulation and Optimization Study for Magnetic Coupler of Static Electric Vehicle Wireless Power Transfer Systems," in *Proc. 22nd Int. Conf. Elect. Mach. Syst.*, Harbin, China, Aug. 2019, pp. 1–4.

[86] Qualcomm Halo, "documents about Qualcomm Halo™ technology" Available: https://www.qualcomm.com/products/halo. [Accessed 21 06 2018].

[87] A. Tejeda, C. Carretero, J. T. Boys and G. A. Covic, "Ferrite-Less Circular Pad With Controlled Flux Cancelation for EV Wireless Charging," *IEEE Trans. Power Electron.*, vol. 32, no. 11, pp. 8349-8359, Nov. 2017.

[88] M. Moghaddami, A. Anzalchi, A. Moghadasi and A. Sarwat, "Pareto optimization of circular power pads for contactless electric vehicle battery charger," in *Proc. 51th IEEE Ind. Appl. Soc. Gen. Meeting*, Portland, OR, 2016, pp. 1-6.

[89] H. Kim et al., "Coil Design and Measurements of Automotive Magnetic Resonant Wireless Charging System for High-Efficiency and Low Magnetic Field Leakage," *IEEE Trans.Microw. Theory Techn.*, vol. 64, no. 2, pp. 383-400, Feb. 2016.

[90] S. Samanta and A. K. Rathore, "A New Inductive Power Transfer Topology Using Direct AC–AC Converter With Active Source Current Waveshaping," *IEEE Trans. Power Electron.*, vol. 33, no. 7, pp. 5565-5577, July 2018.

[91] A. Kamineni, M. J. Neath, A. Zaheer, G. A. Covic and J. T. Boys, "Interoperable EV Detection for Dynamic Wireless Charging With Existing Hardware and Free Resonance," *IEEE Trans. Transport. Electrific.*, vol. 3, no. 2, pp. 370-379, June 2017.

[92] V. Shevchenko, O. Husev, R. Strzelecki, B. Pakhaliuk, N. Poliakov and N. Strzelecka, "Compensation Topologies in IPT Systems: Standards, Requirements, Classification, Analysis, Comparison and Application," in *IEEE Access*, vol. 7, pp. 120559-120580, 2019.

[93] W. Li, H. Zhao, S. Li, J. Deng, T. Kan, C. C. Mi, " Integrated LCC compensation topology for wireless charger in electric and plug-in electric vehicles ", *IEEE Trans. Ind. Electron.*, vol. 62, no. 7, pp. 4215-4225, Jul. 2015.

[94] W. Zhang and C. C. Mi, "Compensation Topologies of High-Power Wireless Power Transfer Systems," *IEEE Trans. Veh. Technol.*, vol. 65, no. 6, pp. 4768–4778, Jun. 2016.

[95] I. Ortego-Isasa, K. P. Benli, F. Casado, J. I. Sancho and D. Valderas, "Topology Analysis of Wireless Power Transfer Systems Manufactured Via Inkjet Printing Technology," *IEEE Trans. Ind. Electron.*, vol. 64, no. 10, pp. 7749-7757, Oct. 2017.

[96] Chwei-Sen Wang, G. A. Covic and O. H. Stielau, "Power transfer capability and bifurcation phenomena of loosely coupled inductive power transfer systems," *IEEE Trans. Ind. Electron.*, vol. 51, no. 1, pp. 148-157, Feb. 2004.

[97] J. Lee, D. Woo, S. Ryu, B. Lee and H. Kim, "Practical bifurcation criteria considering coil losses and compensation topologies in inductive power transfer systems," in *Proc. IEEE Int. Telecommun. Energy Conf.*, Osaka, 2015, pp. 1-6.

[98] J. Acero, J. Serrano, C. Carretero, I. Lope and J. M. Burdío, "Analysis and design of tubular coils for wireless inductive power transfer systems," in *Proc. IEEE Appl. Power Electron. Conf. Expo. (APEC)*, Tampa, FL, 2017, pp. 848-854.

[99] Z. Pantic and S. Lukic, "Computationally-Efficient, Generalized Expressions for the Proximity-Effect in Multi-Layer, Multi-Turn Tubular Coils for Wireless Power Transfer Systems," *IEEE Trans. Magn.*, vol. 49, no. 11, pp. 5404-5416, Nov. 2013.

[100] Y. Tang, H. Ma, D. J. Thrimawithana and U. K. Madawala, "Copper foil windings for WPT systems," in *Proc. IEEE PELS Workshop Emerg. Technol. Wireless Power (WoW)*, Chongqing, 2017, pp. 167-162.

[101] J. M. Miller and A. Daga, "Elements of Wireless Power Transfer Essential to High Power Charging of Heavy Duty Vehicles," *IEEE Trans. Transport. Electrific.*, vol. 1, no. 1, pp. 26-39, June 2015.

[102] New England Wire Technologies. *Tables of Round Litz Cable* [Online]. Available: https://www.newenglandwire.com/litz-wire-do-you-need-a-serve/.

[103] R. Bosshard, Multi-Objective Optimization of Inductive Power Transfer Systems for EV Charging. Zürich, Switzerland: ETH Zurich, 2015.

[104] J. Kim et al., "Coil design and shielding methods for a magnetic resonant wireless power transfer system," *Proc. IEEE*, vol. 101, no. 6, pp. 1332–1342, Jun. 2013.

[105] S. Y. Choi, B. W. Gu, S. W. Lee, W. Y. Lee, J. Huh and C. T. Rim, "Generalized Active EMF Cancel Methods for Wireless Electric Vehicles," *IEEE Trans. Power Electron.*, vol. 29, no. 11, pp. 5770-5783, Nov. 2014.

[106] S. Kim, H. Park, J. Kim, J. Kim and S. Ahn, "Design and Analysis of a Resonant Reactive Shield for a Wireless Power Electric Vehicle," *IEEE Trans.Microw. Theory Techn.*, vol. 62, no. 4, pp. 1057-1066, April 2014.

[107] D. Barth, B. Klaus and T. Leibfried, "Litz wire design for wireless power transfer in electric vehicles," *IEEE Wireless Power Transf. Conf. (WPTC)*, Taipei, 2017, pp. 1-4.

[108] Y. Bu, S. Endo and T. Mizuno, "Improvement in the Transmission Efficiency of EV Wireless Power Transfer System Using a Magnetoplated Aluminum Pipe," *IEEE Trans. Magn.*, vol. 54, no. 11, pp. 1-5, Nov. 2018.

[109] R. Narayanamoorthi and A. V. Juliet, "Capacitor-Less High-Strength Resonant Wireless Power Transfer Using Open Bifilar Spiral Coil," *IEEE Trans. Appl. Supercond.*, vol. 29, no. 1, pp. 1-8, Jan. 2019.

[110] Y. D. Chung, E. Y. Park,W. S. lee, and J. Y. lee, "Impact investigations and characteristics by strong electromagnetic field of wireless power charging system for electric vehicle under air and water exposure indexes," *IEEE Trans. Appl. Supercond.*, vol. 28, no. 3, Apr. 2018.

[111] D. E. Gaona and T. Long, "Feasibility Analysis of Nanocrystalline Cores for Polarize and Non-Polarized IPT Charging Pads," in *Proc. IEEE Appl. Power Electron. Conf. Expo. (APEC)*, Anaheim, CA, USA, 2019, pp. 1539-1546.

[112] X. Li, J. Lu and W. Water, "Design and Study of Data and Power Wireless Transfer System for UAV," in *Proc. 14th IEEE Conf. Ind. Electron. Appl*, Xi'an, China, 2019, pp. 2043-2048.

[113] M. Mohammad, E. Wodajo, S. Choi and M. Elbuluk, "Modeling and Design of Passive Shield to Limit EMF Emission and to Minimize Shield Loss in Unipolar Wireless Charging System for EV," *IEEE Trans. Power Electron.*, vol. 34, no. 12, pp. 12235-12245, Dec. 2019.

[114] M. Mohammad, M. S. Haque and S. Choi, "A Litz-Wire Based Passive Shield Design to limit EMF Emission from Wireless Charging System,"

in *Proc. IEEE Energy Convers. Congr. Expo. (ECCE)*, Portland, OR, 2018, pp. 97-104.
[115] S. Gyimóthy et al., "Loss Computation Method for Litz Cables With Emphasis on Bundle-Level Skin Effect," *IEEE Trans. Magn.*, vol. 55, no. 6, pp. 1-4, June 2019.
[116] J M. Lu and K. D. T. Ngo, "Analytical Calculation of Proximity-Effect Resistance for Planar Coil With Litz Wire and Ferrite Plate in Inductive Power Transfer," *IEEE Trans. Ind. Appl.*, vol. 55, no. 3, pp. 2984-2991, May-June 2019.
[117] H. Li, R. Banucu and W. M. Rucker, "Accurate and Efficient Calculation of the Inductance of an Arbitrary-Shaped Coil Using Surface Current Model," *IEEE Trans. Magn.*, vol. 51, no. 3, pp. 1-4, March 2015.
[118] J. Mühlethaler, "Modeling and multi-objective optimization of inductive power components", 2012.
[119] S. I. Babic and C. Akyel, "New analytic-numerical solutions for the mutual inductance of two coaxial circular coils with rectangular cross section in air," *IEEE Trans. Magn.*, vol. 42, no. 6, pp. 1661-1669, June 2006.
[120] J. Kim, H. Son, D. Kim, K. Kim and Y. Park, "Efficiency of magnetic resonance WPT with two off-axis self-resonators," in *Proc. IEEE MTT-S Inter. Micro. Workshop Series on Innov. Wireless Power Transm.: Techno., Sys., and App*., Uji, Kyoto, 2011, pp. 127-130.
[121] A. Kurs, A. Karalis, R. Moffatt, J. D. Joannopoulos, P. Fisher, and M. Soljacic, "Wireless power transfer via strongly coupled magnetic resonances", *Sci.exp.* , vol. 317, pp. 83-86, July 2007.
[122] S. Wang and D. G. Dorrell, "Loss Analysis of Circular Wireless EV Charging Coupler," *IEEE Trans. Magn.*, vol. 50, no. 11, pp. 1-4, Nov. 2014.
[123] A. Bingler, S. Bilicz, Z. Badics, S. Gyimóthy and J. Pávó, "Integral Equation Formulations for Modeling Wireless Power Transfer Systems in Close Proximity to Foreign Objects," *IEEE Trans. Magn.*, vol. 55, no. 6, pp. 1-4, June 2019.
[124] T. W. Dawson, J. de Moerloose, and M. A. Stuchly, "Comparison of magnetically induced ELF fields in humans computed by FDTD and scalar potential FD codes," *ACES J.*, vol. 11, pp. 63–71, Nov. 1996.
[125] O. P. Gandhi and J.-Y. Chen, "Numerical dosimetry at power-line frequencies using anatomically based models," *Bioelectromagnetics*, vol. 13, no. S1, pp. 43–60, 1992.
[126] M. Alsayegh, M. Saifo, M. Clemens and B. Schmuelling, "Magnetic and Thermal Coupled Field Analysis of Wireless Charging Systems for Electric Vehicles," *IEEE Trans. Magn.*, vol. 55, no. 6, pp. 1-4, June 2019.
[127] N. Chayopitak and D. G. Taylor, "Thermal analysis of linear variable reluctance motor for manufacturing automation applications," in *Proc. IEEE Int. Conf. Elect. Mach. Drives*, 2005., San Antonio, TX, 2005, pp. 866-873.
[128] M. Moghaddami and A. Sarwat, "Time-Dependent Multi-Physics Analysis of Inductive Power Transfer Systems," " in *Proc. IEEE Transp. Electrific. Conf. Expo (ITEC)*, Long Beach, CA, 2018, pp. 130-134.
[129] Engineering Simulation & 3D Design Software, ANSYS fluids, [Online]. Available: http://www.ansys.com.
[130] Most T., Will J. (2008) Metamodel of Optimal Prognosis - an automatic approach for variable reduction and optimal metamodel selection. In Proc. Weimarer Optimierungs- und Stochastiktage 5.0, Weimar, Germany, November 20-21, 2008.
[131] optiSLang - Software for CAE-based Robust Design Optimization and FE-analysis, DYNARDO, Weimar, [Online]. Available: www.dynardo.de.
[132] M. G. S. Pearce, G. A. Covic and J. T. Boys, "Robust Ferrite-Less Double D Topology for Roadway IPT Applications," *IEEE Trans. Power Electron.*, vol. 34, no. 7, pp. 6062-6075, July 2019.
[133] T. Sato, K. Watanabe, and H. Igarashi, "Multimaterial topology optimization of electric machines based on normalized Gaussian network," *IEEE Trans. Magn.*, vol. 51, no. 3, 2015.
[134] Y. Otomo and H. Igarashi, "A 3-D Topology Optimization of Magnetic Cores for Wireless Power Transfer Device," *IEEE Trans. Magn.*, vol. 55, no. 6, pp. 1-5, June 2019.
[135] S. Doi, H. Sasaki and H. Igarashi, "Multi-Objective Topology Optimization of Rotating Machines Using Deep Learning," *IEEE Trans. Magn.*,vol. 55, no. 6, pp. 1-5, June 2019.
[136] F. Lu, H. Zhang, H. Hofmann and C. C. Mi, "An Inductive and Capacitive Combined Wireless Power Transfer System With LC-Compensated Topology," *IEEE Trans. Power Electron.*, vol. 31, no. 12, pp. 8471-8482, Dec. 2016.
[137] B. Luo, T. Long, R. Mai, R. Dai, Z. He and W. Li, "Analysis and design of hybrid inductive and capacitive wireless power transfer for high-power applications," *IET Power Electron*., vol. 11, no. 14, pp. 2263-2270, 27 11 2018.
[138] A. J. Sorgdrager, R. Wang and A. J. Grobler, "Multiobjective Design of a Line-Start PM Motor Using the Taguchi Method," *IEEE Trans. Ind. Appl.*, vol. 54, no. 5, pp. 4167-4176, Sept.-Oct. 2018.

Sampath Jayalath (M'20) received the B.Eng. (Hons.) degree in electronic engineering from Sheffield Hallam University, Sheffield, U.K, in 2013, and the M.Sc. degree in electrical engineering from the University of Cape Town (UCT), Cape Town, South Africa. He is currently with the Department of Electrical Engineering, University of Cape Town, where he is a Lecturer. His research interests include filter design, digital control of power converters, and inductive power transfer.

Azeem Khan (SM'13) received the BSc Eng, MSc and PhD degrees in Electrical Engineering from the University of Cape Town, South Africa. He worked previously at the Electricity Utility in South Africa, Eskom, as a Maintenance Engineer and System Engineer on the turbine and generator control systems. He is currently with the Department of Electrical Engineering at the University of Cape Town in South Africa, where he is a Professor. His research interests are in permanent magnet machine design, and control of renewable energy systems.